

Determination of pion and kaon fragmentation functions including spin asymmetries data in a global analysis

M. Soleymaninia,^{1,2,*} A. N. Khorramian,^{1,2,3,†} S. M. Moosavi Nejad,^{4,2,‡} and F. Arbabifar^{1,2,§}

¹*Faculty of Physics, Semnan University, 35131-19111 Semnan, Iran*

²*School of Particles and Accelerators, Institute for Research in Fundamental Sciences (IPM), P.O. Box 19395-5531, Tehran, Iran*

³*Stanford Institute for Theoretical Physics and Department of Physics, Stanford University, Stanford, California 94305-4060, USA*

⁴*Faculty of Physics, Yazd University, P.O. Box 89195-741, Yazd, Iran*

(Received 10 June 2013; published 20 September 2013; corrected 22 January 2014)

We present a new functional form of pion and kaon fragmentation functions up to next-to-leading order obtained through a global fit to single-inclusive electron-positron annihilation data, and also employ the semi-inclusive deep inelastic scattering asymmetry data from HERMES and COMPASS to determine fragmentation functions. We also apply very recent electron-positron annihilation data from *BABAR* and *Belle* at $\sqrt{s} = 10.54$ GeV and $\sqrt{s} = 10.52$ GeV, respectively. In this analysis we consider the impression of semi-inclusive deep inelastic scattering asymmetry data on the fragmentation functions, where the produced hadrons of different electric charge are identified. We break the symmetry assumption between the quark and antiquark fragmentation functions for favored partons by using the asymmetry data. The results of our analysis are in good agreement with electron-positron annihilation data and also with all the semi-inclusive deep inelastic scattering asymmetry data. We also apply the obtained fragmentation functions to predict the scaled-energy distribution of π^+/K^+ inclusively produced in top-quark decays at next-to-leading order using the zero-mass variable-flavor-number scheme, exploiting the universality and scaling violations of fragmentation functions.

DOI: [10.1103/PhysRevD.88.054019](https://doi.org/10.1103/PhysRevD.88.054019)

PACS numbers: 13.87.Fh, 13.60.Hb, 13.66.Bc, 13.85.Ni

I. INTRODUCTION

In high-energy processes at the Relativistic Heavy Ion Collider (RHIC) and the LHC, the QCD predictions of cross sections have a very important role. In the general case the parton distribution functions (PDFs) of initial hadrons, parton-level differential cross sections, and fragmentation functions are three necessary ingredients to calculate cross sections. Fragmentation functions (FFs) form the non-perturbative component of the hard-scattering process and describe the transition of a parton into the outgoing hadron.

FFs are important for model-independent predictions of the cross sections at the LHC in which a hadron is detected in the outgoing products. Interest in FFs has increased in, for example, tests of QCD such as theoretical calculations for recent measurements of inclusive production in proton-proton collisions at RHIC, and in investigating the origin of the proton spin. In the naive parton model the FFs are independent of the factorization scale (depending only on the scaling variable z), but in the QCD-improved parton model the scaling violations of FFs are subject to Dokshitzer-Gribov-Lipatov-Altarelli-Parisi (DGLAP) evolution equations [1]. Note that FFs can be extracted from fits to data at intermediate to large momentum fractions.

FFs are studied in electron-positron annihilation, and lepton-hadron and hadron-hadron scattering processes.

Among these, e^+e^- annihilation provides a clean environment to determine the fragmentation densities, but without an initial hadron state one cannot separate quark distributions from antiquark distributions. Since the most precise data from e^+e^- annihilation exists for the production of the lightest charged hadrons (pion, kaon, and proton), we are interested in the fragmentation processes of the partons into the pion and kaon in electron-positron annihilation and semi-inclusive deep inelastic scattering. Fragmentation functions are included in hadron-production processes in electron-positron annihilation, lepton-proton or nucleus scattering, and proton-proton and heavy-ion collisions. Such processes are important in hadron physics for studying and investigating the origin of the proton spin [2,3], and the role of FFs in determining the polarized parton distribution functions was pointed out in Refs. [4–7]. In the present analysis to determine FFs, we consider semi-inclusive deep inelastic scattering (SIDIS) asymmetry data along with the data on e^+e^- annihilation from LEP (ALEPH, DELPHI, and OPAL Collaborations), SLAC (SLD and TPC Collaborations), DESY (TASSO Collaboration), KEK (TOPAZ Collaboration) [8–15], and the very recent *BABAR* and *Belle* data at SLAC and KEKB [16,17], respectively. Other kinds of new analyses were also performed by using these new reported data [18,19].

There are already several theoretical studies on QCD analysis for FFs, which are listed in Ref. [20]; in particular, those using parameterizations were widely obtained by the KKP and AKK Collaborations [21] and Kretzer [22]. As was shown in Ref. [23], there are differences between

*Maryam_soleymaninia@ipm.ir

†Khorramiana@theory.ipm.ac.ir

‡Mmoosavi@yazduni.ac.ir

§Farbabifar@ipm.ir

the fragmentation functions of KKP and Kretzer, and therefore it is convenient to make an error calculation for the fragmentation functions to check the consistency of the results. In this regard, a determination of the FFs and their uncertainties has already been attempted by the HKNS and DSS Collaborations [23,24]. But we have an opportunity to use the asymmetry SIDIS experimental data from HERMES [25] and COMPASS [26,27], which makes this the first attempt to study how the asymmetry SIDIS data affects the determination of FFs and their uncertainties.

Since the decay of the top quark is one of the interesting subjects at the LHC, we shall make theoretical predictions for the energy spectrum of π^+ and K^+ mesons produced in top decay using the FFs obtained from our present work. We will also compare our predictions with the known results of Refs. [23,24,28].

This paper is organized as follows. In Sec. II we explain the hadronization process in electron-positron collisions by introducing the FFs. Double-spin asymmetry in semi-inclusive deep inelastic scattering processes is defined in this section too. In Sec. II B we describe our formalism and parametrization form for pion and kaon fragmentation densities. The global χ^2 minimization for the data is defined in this section as well. We also outline the Hessian method for assessing the neighborhood of the global minimum. In Sec. IV our formalism to predict the energy distribution of π^+ and K^+ in top-quark decay is explained. The full results for the pion and kaon FFs and their uncertainties are listed in Sec. V. We also present a comparison of our results with experimental data and the other models, as well as our predictions of the energy spectrum of outgoing pions and kaons in top-quark decay. Our conclusion is given in Sec. VI. We also provide an Appendix which describes the FORTRAN-code which is available.

II. THEORETICAL FORMALISM FOR FRAGMENTATION FUNCTIONS

The fragmentation functions are related to the low-energy components of the hadron-production processes and they form the nonperturbative aspect of QCD. FFs describe the inclusive emission of a hadron from a parton and they cannot be precisely calculated by theoretical methods at this stage. The perturbative QCD framework is used to study single-inclusive hadron production in e^+e^- annihilation, lepton-nucleon deep inelastic scattering (DIS), and hadron-hadron collisions, where the factorization theorem is a strong tool to study such processes. This theorem states that the cross section can be expressed in terms of perturbatively calculable partonic hard-scattering cross sections, PDFs, and FFs, the last two being related to the low-energy components of QCD processes. The low-energy components of QCD processes are universal and they can be used to make predictions.

In this section, we explain the theoretical framework that is relevant for our global QCD analysis of fragmentation functions.

A. Single-inclusive e^+e^- annihilation

In the single-inclusive e^+e^- annihilation processes,

$$e^+e^- \rightarrow (\gamma, Z) \rightarrow H + X, \quad (1)$$

one should not deal with the uncertainty introduced by PDFs in comparison with the hadron collisions, and so the optimal way to determine FFs is to fit them to experimental data extracted from these processes. In the above process, X stands for the unobserved jets which are produced along with a detected hadron H .

The perturbative QCD framework is used to study hadron production in e^+e^- annihilation, where the factorization theorem is an important tool to study this process. According to the hard-scattering factorization theorem of the parton model [29,30], the cross section can be written as a sum of convolutions of perturbatively calculable partonic hard-scattering cross sections, $d\sigma_a(y, \mu_R, \mu_F)/dy$ [22,31,32], with the nonperturbative fragmentation functions of the hadron H from a parton a , $D_a^H(x, \mu_F)$, as follows:

$$\frac{1}{\sigma_{\text{tot}}} \frac{d\sigma^H}{dz} = \sum_a \int_z^1 \frac{dy}{y} D_a^H\left(\frac{z}{y}, \mu_F\right) \frac{1}{\sigma_{\text{tot}}} \frac{d\sigma_a}{dy}(y, \mu_R, \mu_F), \quad (2)$$

where a stands for one of the partons $a = g, u, \bar{u}, \dots, b, \bar{b}$. We denote the four-momenta of the intermediate gauge boson and the hadron H by q and p_H , respectively, so that $s = q^2$, and the scaling variable z is defined as $z = 2(p_H \cdot q)/q^2$. In the c.m. frame, z is simplified to $z = 2E_H/\sqrt{s}$, which refers to the energy of H scaled to the beam energy. The function $D_a^H(x, \mu_F)$ indicates the probability to find the hadron H from a parton a with the scaled energy fraction x . In equation above, y is defined in analogy to z as $y = 2(p_a \cdot q)/q^2$, where p_a is the four-momentum of the parton a . The renormalization and factorization scales are given by μ_R and μ_F , respectively; one can choose two different values for these scales, but a common choice consists of setting $\mu_R^2 = \mu_F^2 = Q^2$, and we shall adopt this convention in this work.

At next-to-leading order (NLO), the total cross section is described by the $q\bar{q}$ pair-creation subprocesses, $e^+e^- \rightarrow (\gamma, Z) \rightarrow q\bar{q} + (g)$, as

$$\sigma_{\text{tot}} = N_c \sigma_0 \sum_{i=1}^{n_f} (V_{q_i}^2 + A_{q_i}^2) \left[1 + \frac{\alpha_s(\mu)}{2\pi} C_F \frac{3}{2} + \mathcal{O}(\alpha_s^2) \right], \quad (3)$$

where $C_F = (N_c^2 - 1)/(2N_c) = 4/3$ for $N_c = 3$ quark colors, $\sigma_0 = (4\pi\alpha^2/3s)$ is the leading-order total cross section of $e^+e^- \rightarrow \mu^+\mu^-$ for massless muons, n_f is the number of active flavors, $N_c = 3$ is the number of quark colors, and α is the electroweak coupling constant. V_{q_i} and A_{q_i} are the effective vector and axial-vector couplings of the quark q_i to both the intermediate photon and Z boson,

which can be found in Ref. [33]. For small energies, $\sqrt{s} \ll M_Z$, for the summation of squared effective electroweak charges one has $V_{q_i}^2 + A_{q_i}^2 = e_{q_i}^2$, where e_{q_i} is the electric charge of the quark q_i ; see Ref. [33].

In our global analysis of FFs, some of the data sets from the OPAL and ALEPH experiments are in the form of $1/N_{Z \rightarrow \text{Hadron}}(dN^H/dz)$, where N is the number of detected events. This is defined as the ratio of the single-inclusive e^+e^- annihilation cross section (2) in a certain bin of z to the totally inclusive rate, i.e.,

$$\frac{1}{N_{\text{tot}}} \frac{dN^H}{dz} \equiv \frac{1}{\sigma_{\text{tot}}} \frac{d\sigma^H}{dz}. \quad (4)$$

B. Hadronization process in ep collisions and spin asymmetry

Generally, the parton distribution function $q(x, Q^2)$ expresses the probability density to find a parton q in a nucleon carrying a fraction x of the target nucleon momentum at the transfer momentum Q^2 . For the polarized PDFs, we assume that a proton is made of massless partons with positive and negative helicity distributions, and thus the difference

$$\delta q(x, Q^2) = q_+(x, Q^2) - q_-(x, Q^2) \quad (5)$$

demonstrates how much the parton of flavor q represents the proton polarization. Universally, the functional forms of the polarized and unpolarized PDFs are determined by a QCD fit to the experimental data obtained from various interactions. These analyses have been discussed in many recent reviews [2,3,34–52] and new, more precise investigations are still in progress.

In order to cover more kinematics regions in the current analysis we consider the polarized SIDIS process, $\vec{l}(l) + \vec{N}(p_N) \rightarrow l'(l') + H(p_H) + X$, where the hadron H is also detected along with the scattered lepton l' and jets X . This process gives remarkable information concerning the nucleon structure in quite a distinct kinematics which probes different aspects of fragmentation distributions. Moreover, SIDIS data help us to specify the difference between the quark and antiquark distributions in the nucleon by considering outgoing produced hadrons, which is not possible in fully inclusive experiments.

In the polarized SIDIS, the measured double-spin asymmetry $A_1^{N,H}$ can be expressed in terms of the ratio of the polarized and unpolarized structure functions $g_1^{N,H}$ and $F_1^{N,H}$ [43] as

$$A_1^{N,H}(x, z, Q^2) = \frac{g_1^{N,H}(x, z, Q^2)_{\text{NLO}}}{F_1^{N,H}(x, z, Q^2)_{\text{NLO}}}, \quad (6)$$

where z is the scaled energy fraction of the outgoing hadron, Q^2 is the transfer momentum, and x is the Bjorken scaling variable. The indices N and H stand for the different nucleon targets and the outgoing detected hadron, respectively.

In the NLO approximation, the polarized and unpolarized structure functions $g_1^{N,H}$ and $F_1^{N,H}$ in SIDIS processes are presented as (see Ref. [43])

$$2g_1^{N,H}(x, z, Q^2) = \sum_{q,\bar{q}}^{n_f} e_q^2 \left\{ \Delta q(x, Q^2) D_q^H(z, Q^2) + \frac{\alpha_s(Q^2)}{2\pi} \right. \\ \times [\Delta q \otimes \Delta C_{qq}^{(1)} \otimes D_q^H + \Delta q \otimes \Delta C_{gq}^{(1)} \otimes D_g^H \\ \left. + \Delta g \otimes \Delta C_{qg}^{(1)} \otimes D_q^H](x, z, Q^2) \right\} \quad (7)$$

and

$$2F_1^{N,H}(x, z, Q^2) = \sum_{q,\bar{q}}^{n_f} e_q^2 \left\{ q(x, Q^2) D_q^H(z, Q^2) + \frac{\alpha_s(Q^2)}{2\pi} \right. \\ \times [q \otimes C_{qq}^{(1)} \otimes D_q^H + q \otimes C_{gq}^{(1)} \otimes D_g^H \\ \left. + g \otimes C_{qg}^{(1)} \otimes D_q^H](x, z, Q^2) \right\}, \quad (8)$$

where n_f is the number of active flavors, e_q is the electric charge of quark q , α_s is the strong coupling constant, Δq and q are polarized and unpolarized parton densities, and $\Delta C_{ij}^{(1)}(x, z)$ and $C_{ij}^{(1)}(x, z)$ are the polarized and unpolarized NLO Wilson coefficient functions, respectively, presented in Ref. [53]. The corresponding parton FFs, $D_{q,\bar{q}}^H$ and D_g^H , are determined in the present global analysis and play a significant role in the determination of $A_1^{N,H}$.

According to Eq. (6) the double-spin asymmetry $A_1^{N,H}$ depends on the polarized and unpolarized parton distribution functions, so in order to calculate the double-spin asymmetry we need to use the results of available polarized parton distribution function (PPDF) and PDF sets. Here we choose the latest DSSV PPDFs and KKT12 PDFs [3,34]; however, different choices of PPDFs and PDFs do not considerably change our result.

III. QCD ANALYSIS AND PARAMETRIZATION

A. ZM-VFN scheme

In a parton fragmentation function $D_i^H(z, \mu^2)$, z represents the fraction of a parton's momentum carried by a produced hadron, while in a parton distribution $q(x, \mu^2)$, x represents the fraction of a hadron's momentum carried by a constituent parton. In both cases, the QCD parton-model approach would predict z and x distributions that are independent of the factorization scale. Note that similar violations of this scaling behavior occur when QCD corrections are taken into account [29]; in other words, beyond the leading order of perturbative QCD these universal functions are factorization-scale dependent. The z dependence of the fragmentation functions is a nonperturbative aspect of QCD and they are not yet calculable from first principles. However, once they are given at the initial fragmentation scale μ_0 their μ evolution is determined by the DGLAP renormalization group equations [1], which are very similar to those for parton densities. For example, the flavor-singlet evolution equation reads [54]

$$\frac{\partial}{\partial \ln \mu^2} \begin{pmatrix} D_S^H(z, \mu^2) \\ D_g^H(z, \mu^2) \end{pmatrix} = \begin{pmatrix} P_{qq}(z) & P_{gq}(z) \\ P_{qg}(z) & P_{gg}(z) \end{pmatrix} \otimes \begin{pmatrix} D_S^H(z, \mu^2) \\ D_g^H(z, \mu^2) \end{pmatrix}, \quad (9)$$

where $D_S^H(z, \mu^2)$ refers to the singlet function $D_S^H(z, \mu^2) = \sum_q [D_q^H(z, \mu^2) + D_{\bar{q}}^H(z, \mu^2)]$, and the convolution integral \otimes is defined by

$$f(z) \otimes g(z) = \int_z^1 \frac{dy}{y} f(y) g\left(\frac{z}{y}\right). \quad (10)$$

The functions P_{ji} are time-like splitting functions, which are the same as those in deep inelastic scattering at the lowest order but the higher-order terms are different. The third-order contributions (N²LO) to the quark-gluon and gluon-quark time-like splitting functions can be found in Ref. [54]. The evolution equations are essentially the same as in the PDF case, so that the same numerical method can be used to obtain a solution. Also, the flavor nonsinglet evolution equation can be found in Refs. [55–57].

To extract the fragmentation functions from data analysis there are several approaches, and in the present analysis we adapt the zero-mass variable-flavor-number (ZM-VFN) scheme [58]. In this scheme, all quarks are treated as massless particles and the nonzero values of the charm- and bottom-quark masses only enter through the initial conditions of the FFs. The number of active flavors also varies with the factorization scale, where for scales higher than the respective flavor thresholds the quark is active as a parton. This scheme works best for high-energy scales, where $m_Q = 0$ is a good approximation.

We also evaluate $\alpha_s^{(n_f)}(\mu)$ at NLO in the improved-minimal subtraction ($\overline{\text{MS}}$) scheme using

$$\alpha_s^{(n_f)}(\mu) = \frac{1}{b_0 \log(\mu^2/\Lambda^2)} \left[1 - \frac{b_1 \log[\log(\mu^2/\Lambda^2)]}{b_0^2 \log(\mu^2/\Lambda^2)} \right], \quad (11)$$

with

$$b_0 = \frac{33 - 2n_f}{12\pi}, \quad b_1 = \frac{153 - 19n_f}{24\pi^2}, \quad (12)$$

where Λ is the typical QCD scale. We adopt $\Lambda_{\text{QCD}}^{(4)} = 334.0$ MeV [59] for NLO adjusted such that $\alpha_s^{(5)} = 0.1184$ for $M_Z = 91.1876$ GeV [60]. Also, $\Lambda_{\text{QCD}}^{(4)}$ at leading order (LO) is fixed in our fits to 220.0 MeV.

B. Parametrization of fragmentation functions

We parametrize the pion and kaon fragmentation functions at LO and NLO considering the single-inclusive annihilation (SIA) and SIDIS data. At the initial scale μ_0 this parametrization contains the functional form

$$D_i^H(z, \mu_0^2) = N_i z^{\alpha_i} (1-z)^{\beta_i} [1 - e^{-\gamma_i z}], \quad (13)$$

which is a convenient form for the light hadrons. A simple polynomial parametrization with just three parameters (N_i , α_i , and β_i) controls the small- and large- z regions [61]. Accordingly, the power term in z emphasizes the small- z region and the power term in $(1-z)$ restricts the large- z region. We consider the extra term $[1 - e^{-\gamma_i z}]$ to control the medium- z region and to improve the accuracy of the global fit [62]. The free parameters N_i , α_i , β_i , and γ_i are determined by fitting the χ^2 of the SIA and SIDIS data. In the $\overline{\text{MS}}$ scheme, there is an important sum rule for the FFs regarding energy conservation,

$$\int_0^1 dz z \sum_H D_i^H(z, \mu^2) = 1, \quad (14)$$

which means that each parton will surely fragment into some hadron H . Since the summation over all the hadrons cannot be taken practically and the behavior of small values of z is unstable, Eq. (14) cannot be a viable constraint in a global analysis.

The initial scale μ_0 is different for partons. The starting scale for the FFs of the light quarks (u/\bar{u} , d/\bar{d} , s/\bar{s}) and g into π^\pm/K^\pm mesons is $\mu_0^2 = 1$ GeV² and it is taken at $\mu_0^2 = m_c^2$ and $\mu_0^2 = m_b^2$ for charm and bottom quarks [63,64]. We choose $m_c = 1.43$ GeV and $m_b = 4.3$ GeV in our analysis. Then these FFs are evolved to higher scales using the DGLAP group equations in Eq. (9).

In all analyses it is necessary to use different assumptions for various FFs. In our analysis, we take the same fragmentation densities for valence quarks. Since the possibility of π^+/K^+ production from valence or favored quarks is more than that from sea or unfavored quarks, we assume distinct fragmentation functions for the light sea quarks. Because of the mass difference, the different functions are also specified for heavy quarks and we assume the same FFs for a heavy quark and its antiquark, $D_c^H = D_{\bar{c}}^H$ and $D_b^H = D_{\bar{b}}^H$. According to the pion structure $|\pi^+\rangle = |u\bar{d}\rangle$ and the general functional form presented in Eq. (13), for the parton FFs into π^+ one has

$$\begin{aligned} D_{u,\bar{d}}^{\pi^+}(z, \mu_0^2) &= N_u^{\pi^+} z^{\alpha_u^{\pi^+}} (1-z)^{\beta_u^{\pi^+}} [1 - e^{-\gamma_u^{\pi^+} z}], \\ D_{d,\bar{u},s,\bar{s}}^{\pi^+}(z, \mu_0^2) &= N_d^{\pi^+} z^{\alpha_d^{\pi^+}} (1-z)^{\beta_d^{\pi^+}} [1 - e^{-\gamma_d^{\pi^+} z}], \end{aligned} \quad (15)$$

where we impose SU(2) isospin invariance between u and \bar{d} quarks for a pion. Isospin symmetry is also considered for sea quarks of pion fragmentation functions. Gluon and heavy-quark FFs are defined as

$$\begin{aligned} D_g^{\pi^+}(z, \mu_0^2) &= N_g^{\pi^+} z^{\alpha_g^{\pi^+}} (1-z)^{\beta_g^{\pi^+}} [1 - e^{-\gamma_g^{\pi^+} z}], \\ D_{c,\bar{c}}^{\pi^+}(z, m_c^2) &= N_c^{\pi^+} z^{\alpha_c^{\pi^+}} (1-z)^{\beta_c^{\pi^+}} [1 - e^{-\gamma_c^{\pi^+} z}], \\ D_{b,\bar{b}}^{\pi^+}(z, m_b^2) &= N_b^{\pi^+} z^{\alpha_b^{\pi^+}} (1-z)^{\beta_b^{\pi^+}} [1 - e^{-\gamma_b^{\pi^+} z}]. \end{aligned} \quad (16)$$

Considering the constituent quark composition of the kaon, $|K^+\rangle = |u\bar{s}\rangle$, we define the kaon functional form for light partons as follows:

$$\begin{aligned}
D_u^{K^+}(z, \mu_0^2) &= N_u^{K^+} z^{\alpha_u^{K^+}} (1-z)^{\beta_u^{K^+}} [1 - e^{-\gamma_u^{K^+} z}], \\
D_s^{K^+}(z, \mu_0^2) &= N_s^{K^+} z^{\alpha_s^{K^+}} (1-z)^{\beta_s^{K^+}} [1 - e^{-\gamma_s^{K^+} z}], \quad (17) \\
D_{d,\bar{d},\bar{u},s}^{K^+}(z, \mu_0^2) &= N_d^{K^+} z^{\alpha_d^{K^+}} (1-z)^{\beta_d^{K^+}} [1 - e^{-\gamma_d^{K^+} z}].
\end{aligned}$$

We apply a new form of the kaon FF for the strange quark because of its mass compared to the u -quark mass. Kaon fragmentation functions for sea quarks are defined by considering the isospin symmetry between them. Gluon and heavy-quark FFs are defined as follows:

$$\begin{aligned}
D_g^{K^+}(z, \mu_0^2) &= N_g^{K^+} z^{\alpha_g^{K^+}} (1-z)^{\beta_g^{K^+}} [1 - e^{-\gamma_g^{K^+} z}], \\
D_{c,\bar{c}}^{K^+}(z, \mu_c^2) &= N_c^{K^+} z^{\alpha_c^{K^+}} (1-z)^{\beta_c^{K^+}}, \quad (18) \\
D_{b,\bar{b}}^{K^+}(z, \mu_b^2) &= N_b^{K^+} z^{\alpha_b^{K^+}} (1-z)^{\beta_b^{K^+}}.
\end{aligned}$$

In our analysis, the heavy parton parameters γ_c and γ_b affect the χ^2 value. We use Eq. (13) as a functional form for all partons of the pion and our decision to include or omit the term $[1 - e^{-\gamma_i z}]$ for different flavors of kaon FFs is based on getting the best χ^2 . In the reported parameters in Refs. [22–24] some parameters are fixed, i.e., the simple parametrization form is used. In Ref. [23] one of the gluon parameters was fixed for the pion and kaon, and the DSS model [24] uses the simple parametrization for c and b quarks for π^+ and K^+ mesons.

According to the parton structure of $\pi^- (\bar{u}d)$ and $K^- (\bar{u}s)$, the parton fragmentation functions can be calculated for π^- and K^- as

$$D_i^{\pi^-}(z, \mu_0^2) = D_i^{\pi^+}(z, \mu_0^2), \quad D_i^{K^-}(z, \mu_0^2) = D_i^{K^+}(z, \mu_0^2), \quad (19)$$

where $i = u, d, s, c, b$, and for the gluon fragmentation functions we obtain

$$D_g^{\pi^-}(z, \mu_0^2) = D_g^{\pi^+}(z, \mu_0^2), \quad D_g^{K^-}(z, \mu_0^2) = D_g^{K^+}(z, \mu_0^2). \quad (20)$$

C. QCD analysis of experimental data and global minimization of χ^2

The free parameters in the functional forms of the π^+ and K^+ FFs [Eqs. (15)–(18)] are determined by minimizing χ^2 for differential cross section and asymmetry experimental data [i.e., $(1/\sigma_{\text{tot}} \cdot d\sigma/dz)_{\text{exp}}$ and $(A_1^{N,H})_{\text{exp}}$] in x space. The global χ^2 is defined as

$$\chi_{\text{global}}^2 = \sum_n w_n \chi_n^2, \quad (21)$$

where n is the number of the experimental data group and w_n denotes a weight factor for the n th experimental data group. The χ_n^2 is defined as

$$\chi_n^2 = \left(\frac{1 - N_n}{\Delta N_n} \right)^2 + \sum_{j=1}^k \left(\frac{N_n E_j - T_j}{N_n \sigma_j^E} \right)^2, \quad (22)$$

where T_j and E_j are the theoretical and experimental values of $1/\sigma_{\text{tot}} \cdot d\sigma/dz$ for e^+e^- SIA data and $A_1^{N,H}$ for SIDIS data, and σ_j^E is the error of the corresponding experimental value. Here, the summation goes over the k bins of the experimental data. ΔN_n is related to the experimental normalization uncertainty which is reported by the experiments, and N_n corresponds to an overall normalization factor which refers to the experimental data. Usually, N_n is calculated from the first minimization and fixed in the second minimization. In our global fit we take SIA experimental data from LEP (ALEPH, DELPHI, and OPAL Collaborations), SLAC (BABAR, SLD, and TPC Collaborations), DESY (TASSO Collaboration), and KEK (Belle and TOPAZ Collaborations). The energy scales of the experimental data are from 10.52 GeV to 91.2 GeV [8–17]. In the reported data without discrimination of hadron species, authors have distinguished between four cases: fragmentation of u, d , and s quarks, c quarks only, b quarks only, and all five quark flavors (u, d, s, c , and b). These categories are only in the DELPHI and SLD data [9,10,12].

Also, the BABAR and Belle Collaborations [16,17] recently reported inclusive hadron-production cross sections at a center-of-mass energies of 10.54 GeV and 10.52 GeV, respectively. Since the center-of-mass energies are below the threshold to produce a $b\bar{b}$ pair, these data contain a pure $e^+e^- \rightarrow q\bar{q}$ sample, where $q = u, d, s, c$. Although most of the precision e^+e^- annihilation data are limited to results from experiments at LEP and SLAC at the energy scale of the M_Z , large data samples are available from the BABAR and Belle Collaborations at $Q = 10.54$ GeV and $Q = 10.52$ GeV, respectively. In addition, these two collaborations reported the differential cross sections at $z > 0.7$. We also provide SIDIS experimental data for $A_1^{p,\pi^+}, A_1^{p,\pi^-}, A_1^{d,\pi^+}, A_1^{d,\pi^-}, A_1^{p,K^+}, A_1^{p,K^-}, A_1^{d,K^+}$, and A_1^{d,K^-} from HERMES05 [25], COMPASS09 [26], and COMPASS10 [27]. The energy scales of SIDIS experimental data are from 1.16 GeV² to 55.60 GeV².

In each collaboration, small- z data were excluded since the splitting functions in evolution equations lead to negative FFs in their NLO part for $z \ll 1$, and additionally mass corrections are more important in this region. So we exclude regions where mass corrections and the singular small- z behavior of the splitting functions are effective. $z > 0.1$ is used for data which have $\sqrt{s} < M_Z$ and $z > 0.05$ is used for data which have $\sqrt{s} = M_Z$.

D. Neighborhood of the global minimum and the Hessian method

In recent years, the assessment of uncertainties has seen significant progress in the QCD analysis of PDFs and FFs [65–67], and among the different approaches the Lagrange multiplier technique (LM) and the Hessian method are the most reliable ones. While LM avoids any approximations or assumptions about the effect of the χ^2 on the parameters, its

only drawback is that its calculation is slow because it needs separate minimizations for each of the parameters.

Since we use the Hessian or error matrix approach in our analysis, we will explain the outline of this method. The basic assumption of the Hessian approach is a quadratic expansion of the χ^2 in the fit parameters a_i near the global minimum,

$$\Delta\chi^2 \equiv \chi^2 - \chi_{\min}^2 = \sum_{i,j=1}^n H_{ij}(a_i - a_i^0)(a_j - a_j^0), \quad (23)$$

with

$$H_{ij} = \frac{1}{2} \frac{\partial^2 \chi^2}{\partial a_i \partial a_j} \Big|_{\min}, \quad (24)$$

where H_{ij} are the elements of the Hessian matrix. Since the Hessian matrix and its inverse ($C \equiv H^{-1}$)—which is the error matrix—are symmetric, they have a set of n *orthogonal* eigenvectors v_{ik} with eigenvalues λ_k ,

$$\sum_{j=1}^n C_{ij} v_{jk} = \lambda_k v_{ik}, \quad (25)$$

$$\sum_{i=1}^n v_{ij} v_{ik} = \delta_{jk}. \quad (26)$$

The parameter variation around the global minimum can be expanded in a basis of eigenvectors and eigenvalues; that is,

$$a_i - a_i^0 = \sum_{k=1}^n e_{ik} z_k, \quad (27)$$

where $e_{ik} \equiv \sqrt{\lambda_k} v_{ik}$. Using Eqs. (26) and (27), it can be shown that the expansion of the χ^2 in the fit parameters a_i near the global minimum (23) reduces to

$$\chi^2 = \chi_{\min}^2 + \sum_{k=1}^n z_k^2, \quad (28)$$

where $\sum_{k=1}^n z_k^2 \leq T^2$ is the interior of a sphere of radius T . The eigenvector sets S_k^\pm are defined by choosing $T = (\Delta\chi^2)^{1/2}$ and the corresponding positive and negative of eigenvector directions are defined as follows:

$$z_i(S_k^\pm) = \pm T \delta_{ik}. \quad (29)$$

Using the last equation, the a_i parameters that specify the eigenvector basis sets S_k^\pm at a fixed value of α_S are given by

$$a_i(S_k^\pm) = a_i^0 \pm T e_{ik}. \quad (30)$$

In the standard parameter-fitting criterion, the errors are given by the choice of the tolerance $T = 1$. Also, we can determine the size of uncertainties by applying the Hessian method based on the correspondence between the confidence level P and $\Delta\chi^2$ with the number of fitting parameters N ,

$$P = \int_0^{\Delta\chi^2} \frac{1}{2\Gamma(N/2)} \left(\frac{x}{2}\right)^{\frac{N}{2}-1} \exp\left(-\frac{x}{2}\right) dx, \quad (31)$$

where we get $P = 0.68$ as the confidence level, and $\Delta\chi^2 = 22.43$ and $\Delta\chi^2 = 24.58$ are obtained for the pion and kaon, respectively.

The uncertainty on the quantity $F(a_i)$, which is an attributive function of the input parameters obtained in the QCD fit procedure at the scale Q_0 , is obtained by applying the simple Hessian method,

$$\Delta F = T \sqrt{\sum_{i,j=1}^n \frac{\partial F}{\partial a_i} C_{ij} \frac{\partial F}{\partial a_j}}. \quad (32)$$

E. The method of error calculation

According to Eqs. (15)–(18) the evolved fragmentation functions for the pion and kaon are attributive functions of the input parameters which are calculated from the fit. Their standard linear errors are given by Gaussian error propagation. If $D_i^H(z; Q^2)$ is the evolved fragmentation density at Q^2 then the Gaussian error propagation is defined as

$$[\delta D_i^H(z)]^2 = \Delta\chi^2 \sum_{j,k} \frac{\partial D_i^H(z, a_j)}{\partial a_j} (H_{jk})^{-1} \frac{\partial D_i^H(z, a_k)}{\partial a_k}, \quad (33)$$

where $\Delta\chi^2$ is the allowed variation in χ^2 , and $a_j|_{j=1}^n$ are free parameters, where n is the number of parameters in the global fit. Also, H_{jk} is the Hessian or covariance matrix of the parameters determined in the QCD analysis at the initial scale Q_0^2 , and it is defined in Eq. (24).

Consequently, we can calculate the uncertainties of any FFs by using the Hessian or covariance matrix based on the Gaussian method at any value of Q^2 by the QCD evolution. More information and a detailed discussion can be found in Refs. [23,68,69].

IV. INCLUSIVE π^+/K^+ -MESON PRODUCTION IN TOP-QUARK DECAY

Nowadays, the LHC at CERN is a superlative machine for producing top-quark pairs; at the design energy $\sqrt{S} = 14$ TeV and design luminosity $\mathcal{L} = 10^{34} \text{ cm}^{-2} \text{ s}^{-1}$ in each of the four experiments it is expected to produce about 90 million top-quark pairs per year [70]. This large volume of events will allow for the determination of the properties of the top quark—such as its mass m_t , branching fractions, and matrix elements V_{tq} of the Cabibbo-Kobayashi-Maskawa [71]—with high precision. Because of its large mass, the top quark decays so rapidly that it has no time to hadronize, and due to the fact that $|V_{tb}| \approx 1$ top quarks almost decay to bottom quarks via the decay mode $t \rightarrow bW^+$ in the standard model. Bottom quarks also hadronize—via $b \rightarrow H + X$ —before they decay, and thus the decay mode $t \rightarrow HW^+ + X$ is of prime importance, where H refers to the detected outgoing hadron. Of particular interest at the LHC is the study of the scaled energy distributions of outgoing hadrons.

In this section, we study the energy spectrum of the inclusive light mesons including the π^+ and K^+ in top-quark decay, working in the ZM-VFN scheme.

TABLE I. Fit parameters for the parton FFs into the charged pion (π^+) at LO, $D_i^{\pi^+}(z, \mu_0)$. The starting scale is taken to be $\mu_0^2 = 1 \text{ GeV}^2$ for light partons and gluons, and $\mu_0^2 = m_c^2$ and $\mu_0^2 = m_b^2$ for c and b quarks.

Flavor i	N_i	α_i	β_i	γ_i
u, \bar{d}	0.841 ± 0.435	-2.041 ± 0.417	0.803 ± 0.284	1.170 ± 0.789
\bar{u}, d, s, \bar{s}	2.509 ± 1.143	-1.514 ± 0.269	4.610 ± 1.083	2.123 ± 1.189
c, \bar{c}	1.059 ± 0.788	-1.918 ± 0.364	3.325 ± 1.060	1.697 ± 1.447
b, \bar{b}	1.062 ± 0.596	-2.043 ± 0.218	5.902 ± 1.328	1.750 ± 1.044
g	59.993 ± 10.523	0.939 ± 1.961	5.801 ± 5.394	1.219 ± 3.508

TABLE II. Values of fit parameters for the π^+ meson at NLO in the starting scale.

Flavor i	N_i	α_i	β_i	γ_i
u, \bar{d}	1.049 ± 0.563	-1.916 ± 0.421	0.977 ± 0.304	0.964 ± 0.65
\bar{u}, d, s, \bar{s}	9.968 ± 7.441	-0.516 ± 0.481	5.952 ± 1.565	1.898 ± 1.885
c, \bar{c}	0.946 ± 0.859	-1.723 ± 0.451	3.590 ± 1.280	1.947 ± 1.981
b, \bar{b}	0.869 ± 0.550	-2.059 ± 0.234	5.803 ± 1.460	1.561 ± 1.054
g	219.507 ± 44.789	1.073 ± 0.362	7.505 ± 1.140	2.142 ± 1.411

TABLE III. Fit parameters for the parton FFs into the charged kaon (K^+) at LO [$D_i^{K^+}(z, \mu_0)$] in the starting scale.

Flavor i	N_i	α_i	β_i	γ_i
u	4.415 ± 5.203	-0.388 ± 0.315	1.486 ± 0.725	0.412 ± 0.513
\bar{s}	29.284 ± 15.300	1.395 ± 1.865	2.524 ± 1.293	0.848 ± 2.413
\bar{u}, d, \bar{d}, s	6.231 ± 3.877	-0.398 ± 0.106	6.273 ± 2.337	2.435 ± 2.168
c, \bar{c}	4.853 ± 3.343	0.245 ± 0.411	4.530 ± 1.090	\dots
b, \bar{b}	8.324 ± 2.947	0.076 ± 0.084	8.841 ± 1.836	\dots
g	1.309 ± 3.529	8.871 ± 4.530	0.293 ± 2.44	0.165 ± 2.732

TABLE IV. Values of fit parameters for the K^+ meson at NLO in the starting scale.

Flavor i	N_i	α_i	β_i	γ_i
u	0.660 ± 0.156	-1.584 ± 0.342	0.858 ± 0.227	0.390 ± 0.107
\bar{s}	17.769 ± 7.775	0.708 ± 0.390	2.479 ± 0.316	0.665 ± 0.218
\bar{u}, d, \bar{d}, s	6.467 ± 1.587	0.028 ± 0.547	7.338 ± 0.819	3.299 ± 1.282
c, \bar{c}	7.217 ± 1.013	0.550 ± 0.113	5.366 ± 0.314	\dots
b, \bar{b}	14.675 ± 3.227	0.293 ± 0.080	10.882 ± 0.943	\dots
g	2.383 ± 0.381	5.714 ± 0.696	0.892 ± 0.085	53542.030 ± 5.859

We wish to study the inclusive production of a light meson in the decay process

$$t \rightarrow b + W^+(g) \rightarrow \pi^\pm / K^\pm + X, \quad (34)$$

where X stands for the unobserved final state. The gluon in Eq. (34) contributes to the real radiation at NLO and both the b quark and the gluon may hadronize to the outgoing light mesons. To obtain the energy distribution of light hadrons we use the realistic FFs obtained in our approach.

To study the energy spectrum of the outgoing meson it would be convenient to introduce the scaled energy fractions $x_i = E_i/E_b^{\max}$ ($i = b, g, H$), where H stands

for the light mesons. In the top-quark rest frame, the energy ranges are $0 \leq (E_b, E_g) \leq (m_t^2 - m_W^2)/(2m_t)$ and $m_H \leq E_H \leq (m_t^2 + m_H^2 - m_W^2)/(2m_t)$ [72].

We wish to calculate the partial decay width of the process (34) differential in x_H ($d\Gamma/dx_H$) at NLO in the ZM-VFN scheme. Considering the factorization theorem of QCD [30], the energy distribution of a hadron H can be expressed as the convolution of the parton-level spectrum with the fragmentation densities $D_i^H(z, \mu_F)$, describing the hadronization $i \rightarrow H$,

$$\frac{d\Gamma}{dx_H} = \sum_{i=b,g} \int_{x_i^{\min}}^{x_i^{\max}} \frac{dx_i}{x_i} \frac{d\hat{\Gamma}_i}{dx_i}(\mu_R, \mu_F) D_i^H\left(\frac{x_H}{x_i}, \mu_F\right), \quad (35)$$

where $d\hat{\Gamma}_i/dx_i$ is the parton-level differential width of the process $t \rightarrow i + W^+$ ($i = b, g$), which is extracted from Ref. [72]. Here, μ_F and μ_R are the factorization and renormalization scales, respectively, which are set to $\mu_R = \mu_F = m_t$. The values of all FF parameters are listed in

Tables I, II, III, and IV. Since these FFs are parametrized at the low factorization scale, the extraction of the FFs at each arbitrary scale of energy should be performed using the grids and fortran routines, which are presented in the Appendix, based on solving DGLAP equations.

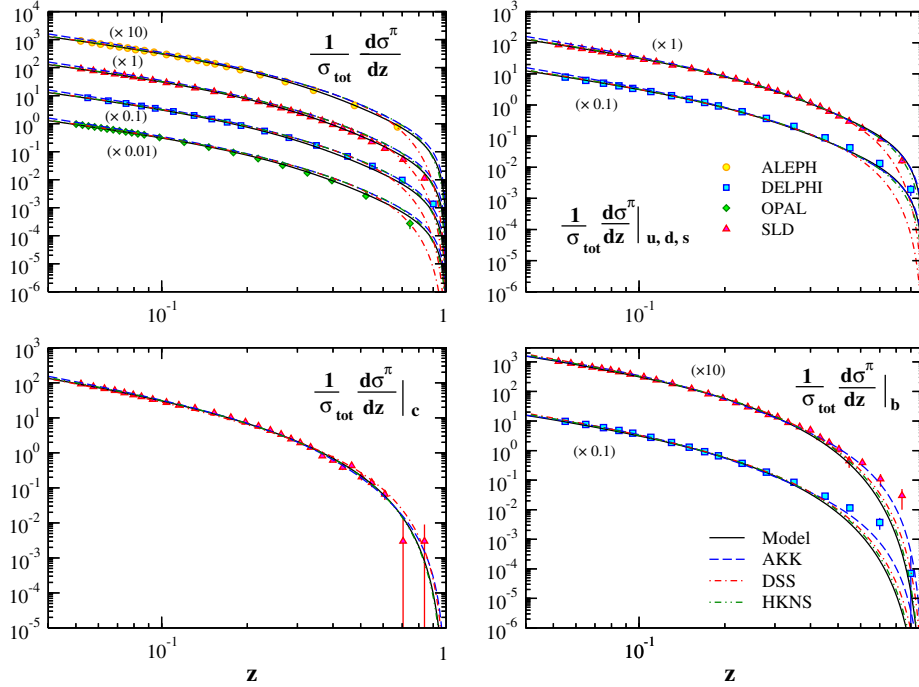


FIG. 1 (color online). Comparison of our NLO results for $\frac{1}{\sigma_{\text{tot}}} \frac{d\sigma^\pi}{dz}$ in total and tagged cross sections with pion production data at $Q^2 = M_Z^2$ by ALEPH, DELPHI, OPAL, and SLD [8–12]. Our model (“Model”) is included for comparison [23,24,28].

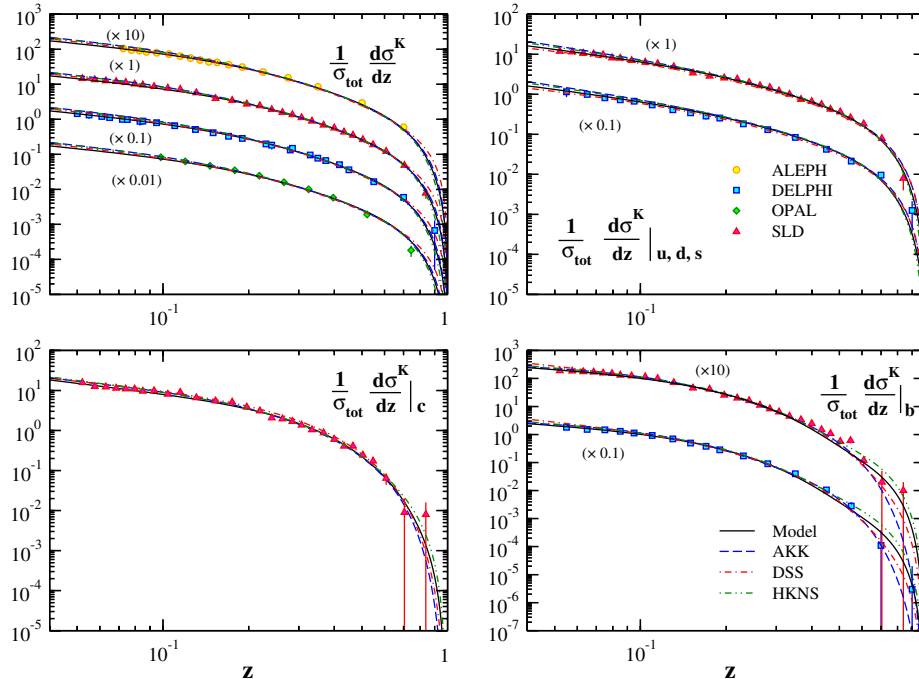


FIG. 2 (color online). Comparison of our NLO results for $\frac{1}{\sigma_{\text{tot}}} \frac{d\sigma^K}{dz}$ in total and tagged cross sections with kaon production data at $Q^2 = M_Z^2$ by ALEPH, DELPHI, OPAL, and SLD [8–12]. Our model (“Model”) is included for comparison [23,24,28].

V. FIT RESULTS

Now we are in a situation to explain our global analysis of the fragmentation functions for the pion and kaon results. We compare our calculated cross section and double-spin asymmetry results with the experimental data and find a good agreement.

According to the last section—where we introduced the experimental data for our fits—we present our results of the optimum fits for the fragmentation parameters of the π^+ and K^+ mesons in the initial scale μ_0 at LO and NLO. We also report χ^2 and normalization fit values for each individual collaboration. On the other hand, we are interested in presenting how much the asymmetry SIDIS data effects the determination of the pion and kaon FFs. Also, the FF comparisons are made with the results obtained in the other FF analyses in Refs. [23,24,28]. We also briefly present the dependance of the global $\Delta\chi^2$ along some random samples of eigenvector directions to illustrate the deviations of the $\Delta\chi^2$ function from the expected quadratic dependence. Finally, we show our prediction for the energy spectra of the pion and kaon as light mesons in top decay.

A. Experimental data and our analysis

The experimental data for inclusive hadron production in SIA covers orders of magnitude from 10.52 GeV to the mass of the Z boson. By adding SIDIS experimental data the range of energy is extended and covers low energies from 1.16 GeV² to 55.60 GeV². In Figs. 1 and 2, using the new functional forms of the FFs, we compare our results for $\frac{1}{\sigma_{\text{tot}}}\frac{d\sigma^i}{dz}$ ($i = \pi$ or K) with the data at $\mu^2 = M_Z^2$ reported by the ALEPH, DELPHI, OPAL, and SLD Collaborations at NLO. In these figures we separate the light, charm, and bottom tagged cross sections, and most of the diagrams show a remarkable agreement between our results and experimental data.

Comparing other FF models in these figures also gives a nice all-around description of our model, where we have used the AKK set [28] that included hadron production data in electron-positron and hadron-hadron scattering data, the DSS set [24] that included electron-positron, lepton-nucleon, and hadron-hadron scattering data, and the HKNS set [23] that included electron-positron data. However, as Fig. 1 shows, due to the largeness of the χ^2 contributions for the SLD and DELPHI b -tagged data

TABLE V. The individual χ^2 values and the fitted normalization at LO for each collaboration and the total χ^2 fit for π^+ .

Collaboration	Data properties	\sqrt{s} GeV	Data points	Relative normalization in fit	$\chi^2(\text{LO})$
Belle [17]	Untagged	10.52	78	0.983	11.5
BABAR [16]	Untagged	10.54	38	0.936	204.5
TPC [14]	Untagged	29	12	0.993	6.4
TASSO [13]	Untagged	34	8	1.051	6.6
	Untagged	44	5	1.051	6.2
TOPAZ [15]	Untagged	58	4	1.013	1.3
ALEPH [8]	Untagged	91.2	22	0.997	28.2
OPAL [11]	Untagged	91.2	22	1.017	35.3
SLD [12]	Untagged	91.2	29	1.012	53.6
	uds tagged	91.2	29	1.012	94.7
	c tagged	91.2	29	1.012	44.8
	b tagged	91.2	29	1.012	90.6
DELPHI [9,10]	Untagged	91.2	17	0.987	9.4
	uds tagged	91.2	17	0.987	7.7
	b tagged	91.2	17	0.987	53.7
HERMES [25]	SIDIS(p, π^+)	1.10–3.23	9	1.051	10.1
	SIDIS(p, π^-)	1.10–3.23	9	1.051	6.6
	SIDIS(d, π^+)	1.10–3.2	9	1.051	11.4
	SIDIS(d, π^-)	1.10–3.2	9	1.051	20.5
COMPASS [26]	SIDIS(d, π^+)	1.07–5.72	10	1.028	3.9
	SIDIS(d, π^-)	1.07–5.72	10	1.028	5.5
COMPASS [27]	SIDIS(p, π^+)	1.07–7.45	12	0.997	10.8
	SIDIS(p, π^-)	1.07–7.45	12	0.997	13.7
<i>TOTAL:</i>			436		736.32
$(\chi^2/\text{d.o.f})$					1.77

TABLE VI. The individual χ^2 values and the fitted normalization at NLO for each collaboration and the total χ^2 fit for π^+ .

Collaboration	Data properties	\sqrt{s} GeV	Data points	Relative normalization in fit	$\chi^2(\text{NLO})$
Belle [17]	Untagged	10.52	78	1.001	12.5
BABAR [16]	Untagged	10.54	38	0.928	138.3
TPC [14]	Untagged	29	12	0.992	5.7
TASSO [13]	Untagged	34	8	1.049	7.9
	Untagged	44	5	1.049	6.9
TOPAZ [15]	Untagged	58	4	1.015	1.6
ALEPH [8]	Untagged	91.2	22	1.001	31.7
OPAL [11]	Untagged	91.2	22	1.020	33.5
SLD [12]	Untagged	91.2	29	1.015	31.7
	<i>uds</i> tagged	91.2	29	1.015	62.3
	<i>c</i> tagged	91.2	29	1.015	26.8
	<i>b</i> tagged	91.2	29	1.015	85.2
DELPHI [9,10]	Untagged	91.2	17	0.991	15.9
	<i>uds</i> tagged	91.2	17	0.991	13.2
	<i>b</i> tagged	91.2	17	0.991	48.8
HERMES [25]	SIDIS(p, π^+)	1.10–3.23	9	1.063	10.3
	SIDIS(p, π^-)	1.10–3.23	9	1.063	4.6
	SIDIS(d, π^+)	1.10–3.2	9	1.063	18.6
	SIDIS(d, π^-)	1.10–3.2	9	1.063	22.3
COMPASS [26]	SIDIS(d, π^+)	1.07–5.72	10	1.071	12.8
	SIDIS(d, π^-)	1.07–5.72	10	1.071	5.61
COMPASS [27]	SIDIS(p, π^+)	1.07–7.45	12	1.011	10.5
	SIDIS(p, π^-)	1.07–7.45	12	1.011	7.6
<i>TOTAL:</i>			436		611.52
<i>($\chi^2/\text{d.o.f}$)</i>					1.47

(see Tables V and VI) some points are outside of the curves. Generally, χ^2 values of the heavy flavors—in particular *b*-tagged data—are larger than the other data (see Tables V, VI, VII, and VIII), and this might be caused to some extent by contaminations from weak decay.

Recent differential cross-section data from the Belle and BABAR Collaborations are included in our analysis. In Fig. 3 our results for the pion and kaon at $Q = 10.52$ GeV and $Q = 10.54$ GeV are compared with these data. Also, the other FF models are compared with Belle and BABAR data and this figure shows a nice agreement between our model and these data.

Figures 4 and 5 present the extracted values of A_1 for the proton and deuteron from the global fit for π^+ , π^- , K^+ , and K^- at NLO in comparison with the SIDIS data from HERMES and COMPASS [25–27]. The extraction of double-spin asymmetry data from the global fit for fragmentation functions is done for the first time, and as is shown the overall agreement of the experimental data sets in the global analysis is great. Some of the theoretical analyses—such as Refs. [3,43]—have used the asymmetry data from DIS and SIDIS to calculate the polarized parton distributions.

B. Fit results for π^+ and K^+ FFs

According to the scenarios defined for the fragmentation functions of π^+ and K^+ mesons at the starting scales, 20 and 22 parameters have to be determined, respectively. These parameters are listed in Tables I and II for π^+ and in Tables III and IV for K^+ at LO and NLO. The initial scales for the $b \rightarrow \pi^+/K^+$ and $c \rightarrow \pi^+/K^+$ FFs are $\mu_0^2 = m_b^2$ and $\mu_0^2 = m_c^2$, respectively, and $\mu_0^2 = 1 \text{ GeV}^2$ is considered for the gluon and light quarks. In Tables V, VI, VII, and VIII, we list all experimental data sets included in our global analysis, discussed in Sec. VA, and the χ^2 values per degree of freedom pertaining to the LO and NLO fits are presented for each collaboration based on data points. The relative normalization in fit for each data set is reported in these tables. Indeed, the global minimization of χ^2 (discussed in Sec. III C) in the global fit considerably improves after taking relative normalization into account.

The π^+ and K^+ fragmentation densities and their uncertainties are presented in Figs. 6 and 7 at $\mu_0^2 = 1 \text{ GeV}^2$ for the gluon and light quarks and $\mu_0^2 = m_c^2$ and $\mu_0^2 = m_b^2$ for *c* and *b* quarks at NLO. We present the FF uncertainties for $\Delta\chi^2 = 1$ and $\Delta\chi^2 = 22.43$ for the pion

TABLE VII. The individual χ^2 values and the fitted normalization at LO for each collaboration and the total χ^2 fit for K^+ .

Collaboration	Data properties	\sqrt{s} GeV	Data points	Relative normalization in fit	χ^2 (LO)
Belle [17]	Untagged	10.52	78	1.060	109.1
BABAR [16]	Untagged	10.54	28	0.992	130.5
TPC [14]	Untagged	29	11	1.063	9.0
TASSO [13]	Untagged	34	4	0.995	0.3
TOPAZ [15]	Untagged	58	3	1.004	0.8
ALEPH [8]	Untagged	91.2	18	1.008	6.1
OPAL [11]	Untagged	91.2	10	0.975	2.7
SLD [12]	Untagged	91.2	29	0.993	19.3
	<i>uds</i> tagged	91.2	29	0.993	61.1
	<i>c</i> tagged	91.2	29	0.993	37.2
	<i>b</i> tagged	91.2	28	0.993	153.6
DELPHI [9,10]	Untagged	91.2	17	1.063	2.3
	<i>uds</i> tagged	91.2	17	1.063	7.4
	<i>b</i> tagged	91.2	17	1.063	11.9
HERMES [25]	SIDIS(d, K^+)	1.22–3.19	9	1.004	7.1
	SIDIS(d, K^-)	1.22–3.19	9	1.004	6.8
COMPASS [26]	SIDIS(d, K^+)	1.07–5.72	10	1.012	7.9
	SIDIS(d, K^-)	1.07–5.72	10	1.012	16.0
COMPASS [27]	SIDIS(p, K^+)	1.07–7.45	12	1.004	10.8
	SIDIS(p, K^-)	1.07–7.45	12	1.004	12.26
<i>TOTAL:</i>			380		612.18
(χ^2 /d.o.f)					1.71

TABLE VIII. The individual χ^2 values and the fitted normalization at NLO for each collaboration and the total χ^2 fit for K^+ .

Collaboration	Data v	\sqrt{s} GeV	Data points	Relative normalization in fit	χ^2 (NLO)
Belle [17]	Untagged	10.52	78	1.029	105.7
BABAR [16]	Untagged	10.54	28	0.974	100.8
TPC [14]	Untagged	29	11	1.041	7.6
TASSO [13]	Untagged	34	4	0.992	0.3
TOPAZ [15]	Untagged	58	3	1.004	0.8
ALEPH [8]	Untagged	91.2	18	1.017	4.9
OPAL [11]	Untagged	91.2	10	0.983	2.8
SLD [12]	Untagged	91.2	29	1.003	19.1
	<i>uds</i> tagged	91.2	29	1.003	67.6
	<i>c</i> tagged	91.2	29	1.003	42.7
	<i>b</i> tagged	91.2	28	1.003	116.5
DELPHI [9,10]	Untagged	91.2	17	1.084	2.6
	<i>uds</i> tagged	91.2	17	1.084	6.9
	<i>b</i> tagged	91.2	17	1.084	11.8
HERMES [25]	SIDIS(d, K^+)	1.22–3.19	9	1.009	6.0
	SIDIS(d, K^-)	1.22–3.19	9	1.009	8.1
COMPASS [26]	SIDIS(d, K^+)	1.07–5.72	10	1.032	7.2
	SIDIS(d, K^-)	1.07–5.72	10	1.032	20.4
COMPASS [27]	SIDIS(p, K^+)	1.07–7.45	12	1.013	6.5
	SIDIS(p, K^-)	1.07–7.45	12	1.013	15.3
<i>TOTAL:</i>			380		551.32
(χ^2 /d.o.f)					1.54

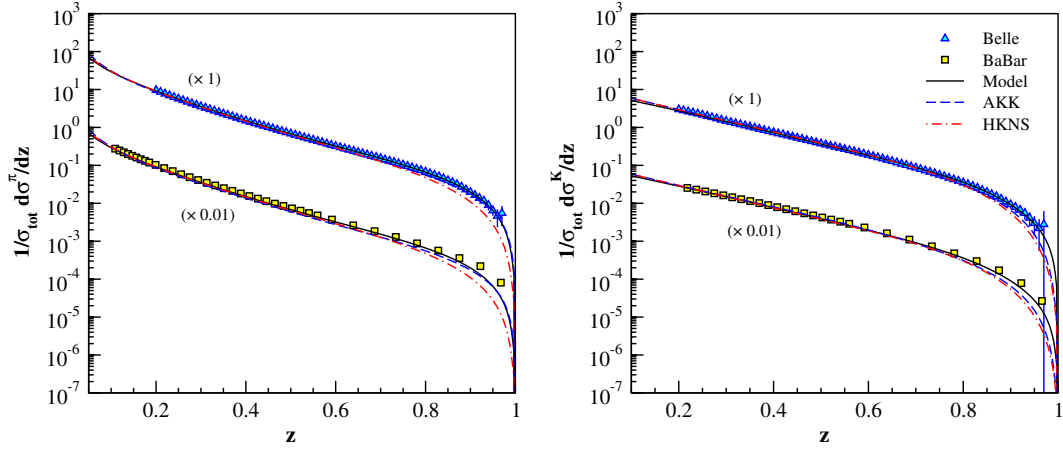


FIG. 3 (color online). Comparison of our NLO results for $\frac{1}{\sigma_{\text{tot}}} \frac{d\sigma^i}{dz}$, ($i = \pi, K$) in total cross sections with pion and kaon production data at $Q = 10.54$ GeV by *BABAR* [16] and $Q = 10.52$ GeV by *Belle* [17]. Our model (“Model”) is also included [23,28].

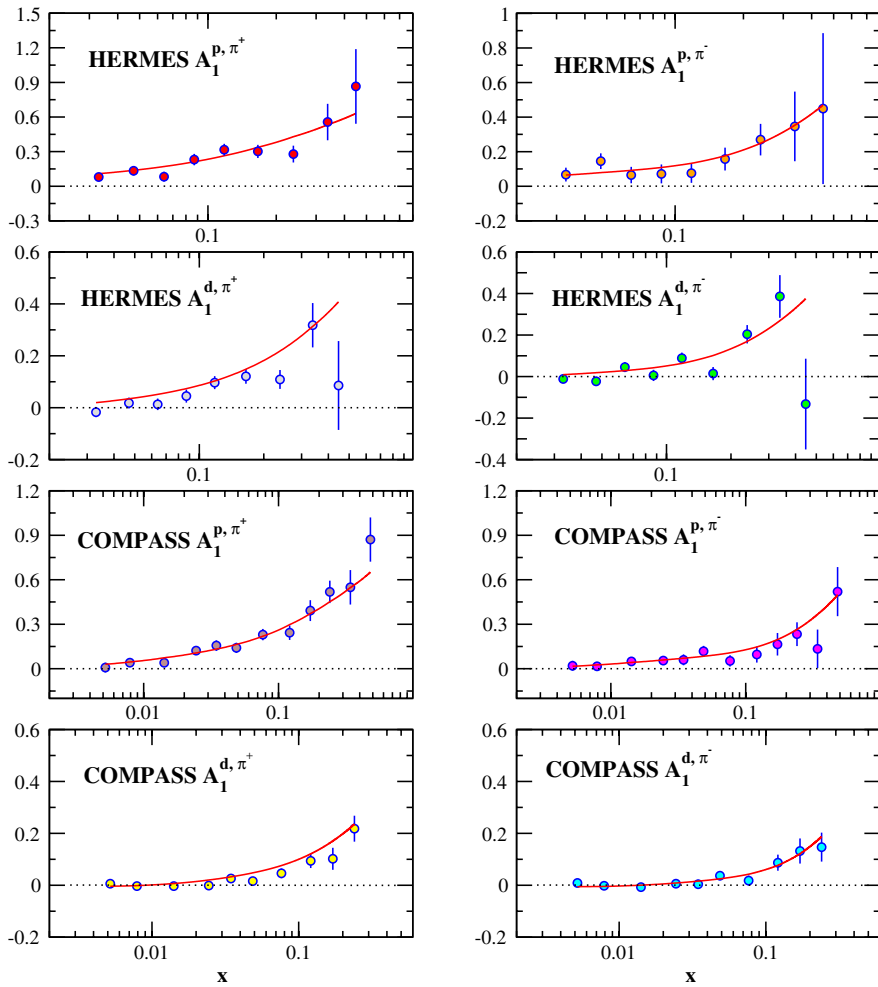


FIG. 4 (color online). Double-spin asymmetry SIDIS data for π^+ and π^- from HERMES and COMPASS [25–27] at measured x and Q^2 and a comparison with the fit results of our global analysis at NLO.

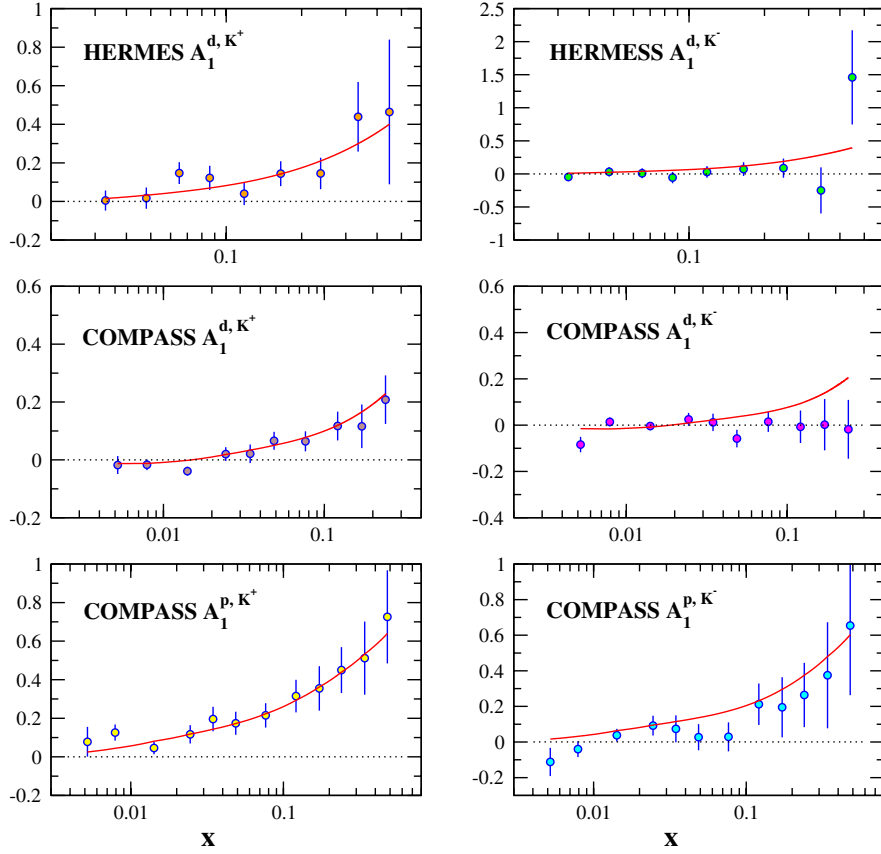


FIG. 5 (color online). Double-spin asymmetry SIDIS data for K^+ and K^- from HERMES and COMPASS [25–27] at measured x and Q^2 and a comparison with the fit results of our global analysis at NLO.

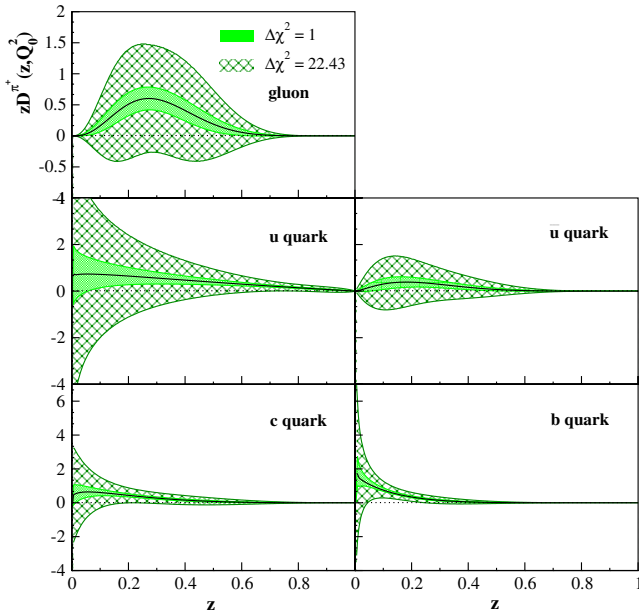


FIG. 6 (color online). Fragmentation densities and their uncertainties are shown for π^+ at $Q_0^2 = 1 \text{ GeV}^2$, m_c^2 , and m_b^2 at NLO. Their uncertainties are presented for $\Delta\chi^2 = 1$ (inner bands) and $\Delta\chi^2 = 22.43$ (outer bands).

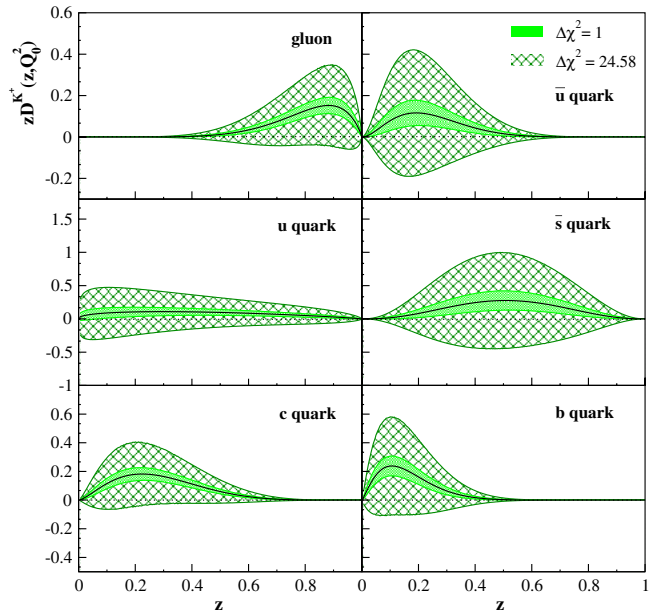


FIG. 7 (color online). Fragmentation densities and their uncertainties are shown for K^+ at $Q_0^2 = 1 \text{ GeV}^2$, m_c^2 , and m_b^2 at NLO. Their uncertainties are presented for $\Delta\chi^2 = 1$ (inner bands) and $\Delta\chi^2 = 24.58$ (outer bands).

and $\Delta\chi^2 = 24.58$ for the kaon in Figs. 6 and 7. The method of error calculation is described in Secs. III D and III E.

To show how different choices of PPDFs from different analyses affect the results, we applied one of the most accurate PPDFs, i.e., KATAO PPDFs [35], which are obtained from a global analysis of DIS data. The comparison of extracted pion and kaon fragmentation functions by including KATAO [35] and DSSV [3] PPDFs are shown in Figs. 8 and 9 at NLO. As can be seen the differences are small and negligible, and these differences become smaller by increasing the energy scaling. Therefore, the different choices of PPDFs do not change our result considerably.

Since we would like to present how effective the asymmetry SIDIS data are at determining the FFs, in Figs. 10 and 11 the FFs for different flavors are presented in two cases at $\mu^2 = M_Z^2$. In the first case we determine FFs by fitting on the SIA and SIDIS asymmetry data. According to the last section, we assume asymmetry between valence or favored fragmentation functions and unfavored fragmentation functions for both the pion and kaon because the possibility of π^+/K^+ production from valence or favored quarks is greater than from sea or unfavored quarks. Moreover, SIDIS data help us to specify the difference between the quark and antiquark distributions in the nucleon by considering outgoing produced hadrons, which is not possible in fully inclusive experiments.

In the second case we calculate FFs by fitting just on the SIA data. Since we omit asymmetric SIDIS data from our fit, the symmetry between the quark and the antiquark is assumed in this case,

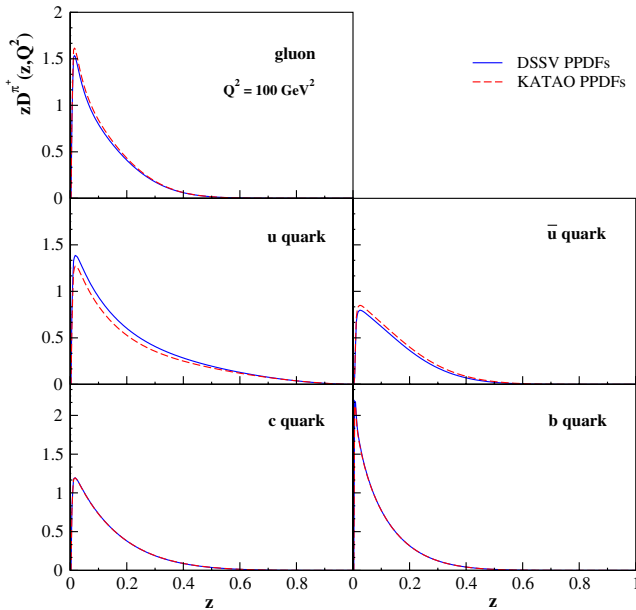


FIG. 8 (color online). Comparison of extracted pion fragmentation functions at $Q^2 = 100 \text{ GeV}^2$ using KATAO [35] and DSSV [3] PPDFs at NLO.

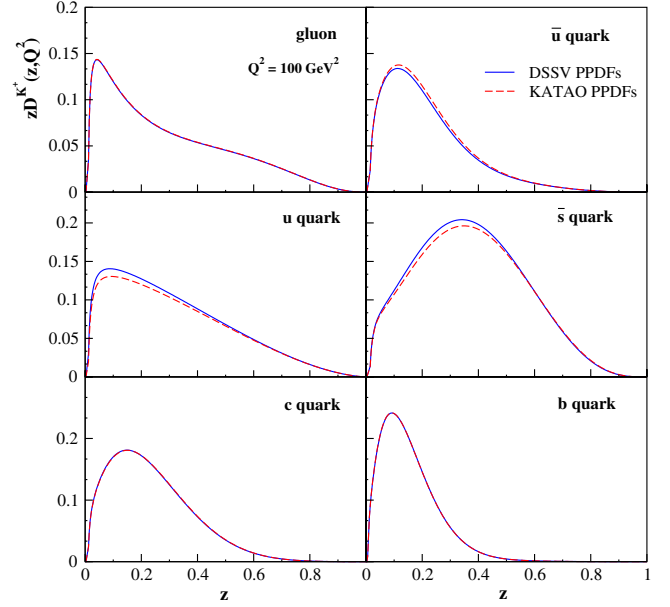


FIG. 9 (color online). Comparison of extracted kaon fragmentation functions at $Q^2 = 100 \text{ GeV}^2$ using KATAO [35] and DSSV [3] PPDFs at NLO.

$$\begin{aligned} D_u^H(z, \mu_0^2) &= D_{\bar{u}}^H(z, \mu_0^2), \\ D_d^H(z, \mu_0^2) &= D_{\bar{d}}^H(z, \mu_0^2), \\ D_s^H(z, \mu_0^2) &= D_{\bar{s}}^H(z, \mu_0^2). \end{aligned} \quad (36)$$

According to Figs. 10 and 11, the SIDIS data are effective on different partons of the FFs. Our results are also compared with the AKK model in these figures.

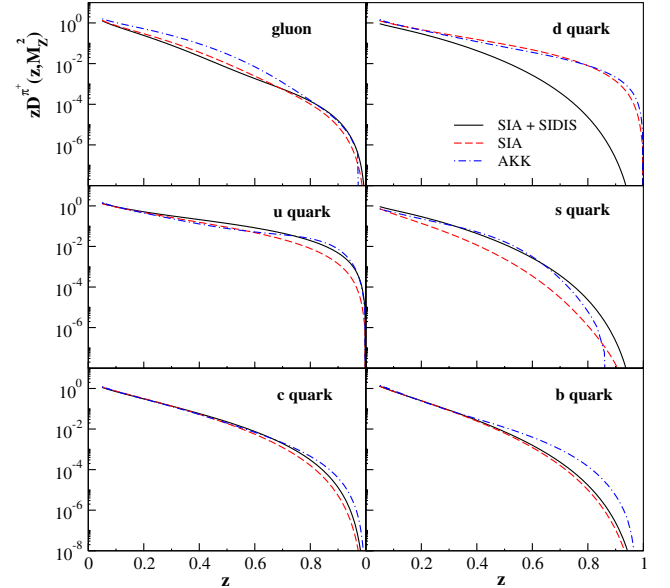


FIG. 10 (color online). Comparison of calculated π^+ FFs at $Q^2 = M_Z^2$ from fitting on SIA data [8–17] with (solid lines) and without (dashed lines) SIDIS data [25–27] at NLO. The results are compared with AKK [28] (dot-dashed lines) too.

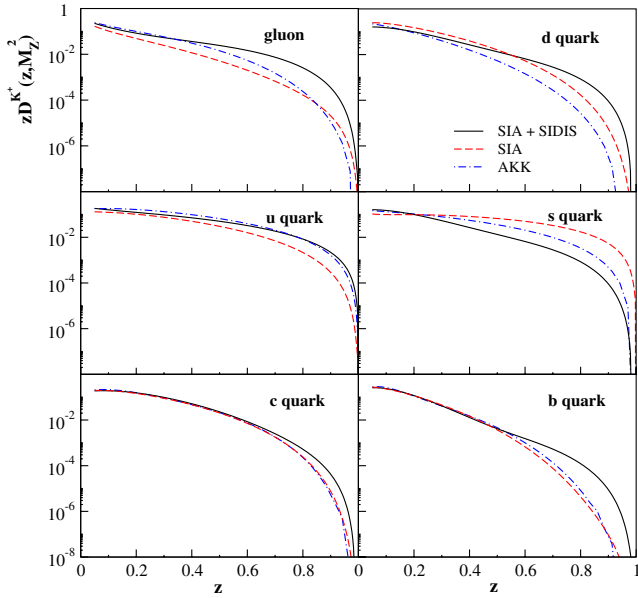


FIG. 11 (color online). Comparison of calculated K^+ FFs at $Q^2 = M_Z^2$ from fitting on SIA data [8–17] with (solid lines) and without (dashed lines) SIDIS data [25–27] at NLO. The results are compared with AKK [28] (dot-dashed lines) too.

We also present the π^+ and K^+ fragmentation densities at the scales $\mu^2 = 10 \text{ GeV}^2$ and $\mu^2 = M_Z^2$ and the ratios of our fragmentation densities to those presented by HKNS, DSS, and AKK [23,24,28] in Figs. 12–15. According to these figures, our FF models’ densities are different in comparison with other models at large z ; this is not unexpected because (according to Figs. 10 and 11), since the effect of the SIDIS data on the FFs at large z is greater than at small z , the ratios in Figs. 12–15 are in much better

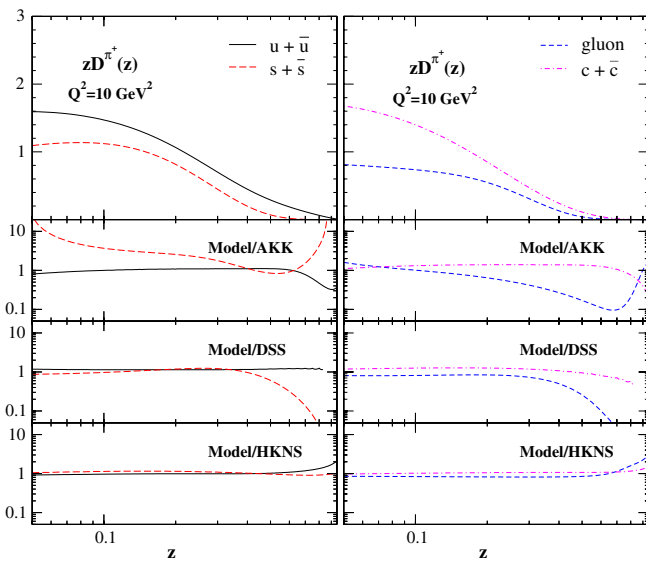


FIG. 12 (color online). Top panels: Fragmentation densities for π^+ at $Q^2 = 10 \text{ GeV}^2$ at NLO. Lower panels: Ratios of our fragmentation densities to those of HKNS, DSS, and AKK [23,24,28].

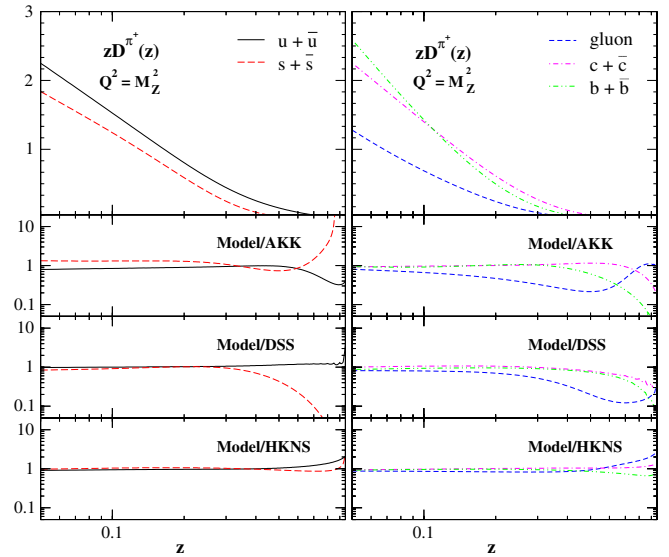


FIG. 13 (color online). Upper panels: fragmentation densities for π^+ at $Q^2 = M_Z^2$ at NLO. Rest panels: ratios of our fragmentation densities to the ones of HKNS, DSS and AKK [23,24,28].

agreement at small z . However, when Q^2 increases the difference between the models decreases.

Since (unlike our assumption) the light-quark functional forms are separated in the AKK analysis due to fully flavor-separated OPAL data, the difference between our FF results and the AKK results is greater than that between our results and the DSS and HKNS results in Figs. 12–15. These data—which are not used in the overall analysis, in contrast to the HKNS analysis—are more difficult to appreciate within perturbative QCD beyond the LO. We then use just the untagged OPAL data, and the light-quark

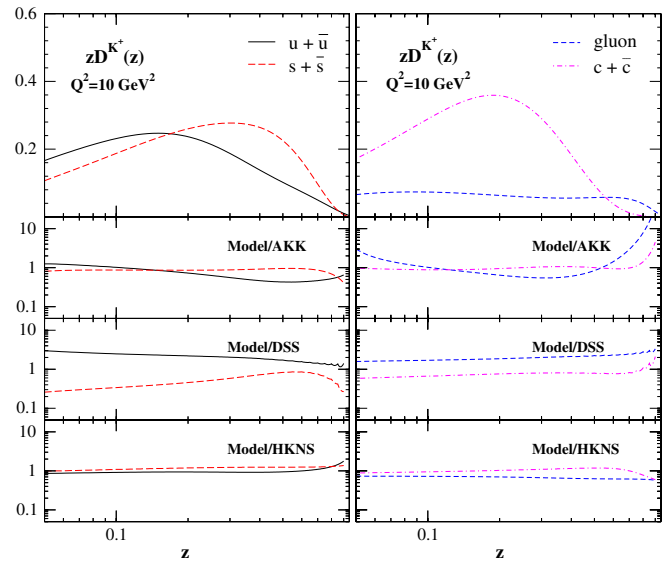


FIG. 14 (color online). Top panels: Fragmentation densities for K^+ at $Q^2 = 10 \text{ GeV}^2$ at NLO. Lower panels: Ratios of our fragmentation densities to those of HKNS, DSS, and AKK [23,24,28].

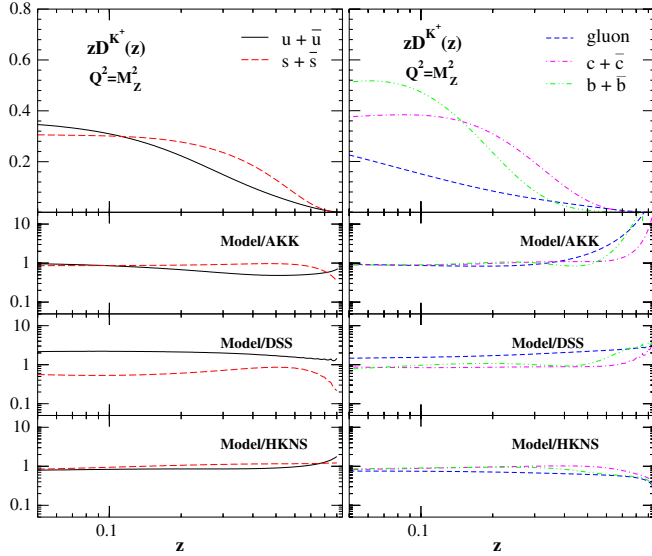


FIG. 15 (color online). Top panels: Fragmentation densities for K^+ at $Q^2 = M_Z^2$ at NLO. Lower panels: Ratios of our fragmentation densities to those of HKNS, DSS, and AKK [23,24,28].

functions are not separated in our analysis, as was done in the DSS and HKNS analyses.

C. Quadratic behavior of $\Delta\chi^2$

According to the Hessian method, which is discussed in Sec. III D, we want to show whether $\Delta\chi^2$ shows the assumed quadratic behavior of the parameters from the best fit. To explore this further, we present the dependance of the global $\Delta\chi^2$ along some random samples of eigenvector directions to illustrate the deviations of the $\Delta\chi^2$ function from the expected quadratic dependence. As can be seen, to exhibit the quadratic approximation in Eq. (23), Figs. 16 and 17 are presented to show the pion and kaon global $\Delta\chi^2$ along some random samples of eigenvector directions. Since the variation range of the fitted parameters is correlated, here only one of the parameters is varied. Figure 16 presents the pion $\Delta\chi^2$ along some random samples of eigenvector directions, with the eigenvalues $k = 6, 9, 16, 19,$ and 20 . In this figure the curve with the eigenvector direction $k = 19$ for the pion shows the most idealistic quadratic behavior, and the curves with $k = 6, 9$ show a deviation from the ideal parabolic behavior curve, $\Delta\chi^2 = T^2$. Figure 17 presents the kaon $\Delta\chi^2$ along some random samples of eigenvector directions, with the eigenvalues $k = 8, 9, 13$ and 17 . To have a best fit we omit the term $[1 - e^{-\gamma_i z}]$ for heavy partons c/\bar{c} and b/\bar{b} in the global analysis of the kaon (see Tables III and IV), which improves the quadratic behavior of $\Delta\chi^2$. More details about the kaon parameters are explained in Sec. III B.

D. Energy spectrum of light mesons in top-quark decay

Now, by having the pion and kaon fragmentation functions in every scale, we make our phenomenological

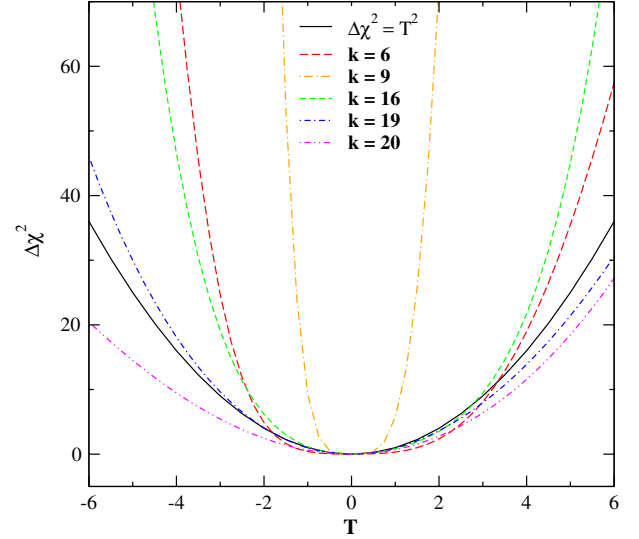


FIG. 16 (color online). Examples of pion $\Delta\chi^2$ deviations from the expected quadratic behavior $\Delta\chi^2 = T^2$ for random sample eigenvector directions.

prediction for the energy spectrum of light mesons in top decay. We adopt from Ref. [60] the input parameter values $G_F = 1.16637 \times 10^{-5} \text{ GeV}^{-2}$, $m_t = 172.0 \text{ GeV}$, and $m_{W^+} = 80.399 \text{ GeV}$. In Figs. 18 and 19, we show our predictions for the size of the NLO corrections and their uncertainties by comparing the relative importance of the $b \rightarrow \pi^+/K^+$ (dashed line) and $g \rightarrow \pi^+/K^+$ (dot-dashed line) fragmentation, on a logarithmic scale. As is seen, the gluon fragmentation leads to an appreciable reduction in the decay rate in the low- x_H region, and for higher values of x_H the $b \rightarrow H$ contribution is dominant. The mass of the light meson is responsible for the appearance of the threshold at

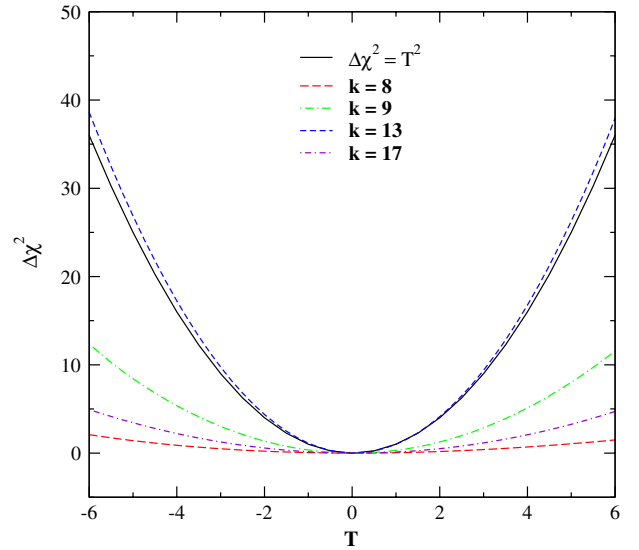


FIG. 17 (color online). Examples of kaon $\Delta\chi^2$ deviations from the expected quadratic behavior $\Delta\chi^2 = T^2$ for random sample eigenvector directions.

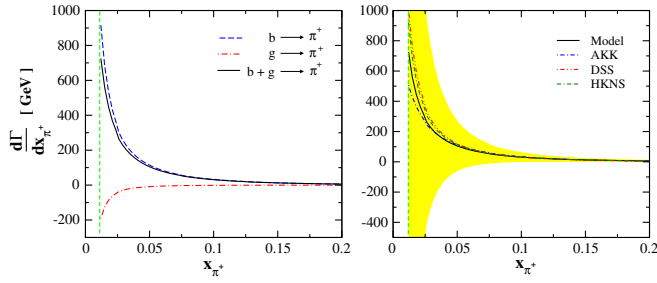


FIG. 18 (color online). Left panel: Energy distribution of the π^+ meson in top decay considering the fragmentation contribution of the b quark (dashed line) and gluon (dot-dashed line) into the π^+ and the total contribution (solid line) at $\mu_F = m_t$. Right panel: Energy distribution and its uncertainty of π^+ considering the FFs obtained by our model, AKK, DSS, and HKNS [23,24,28].

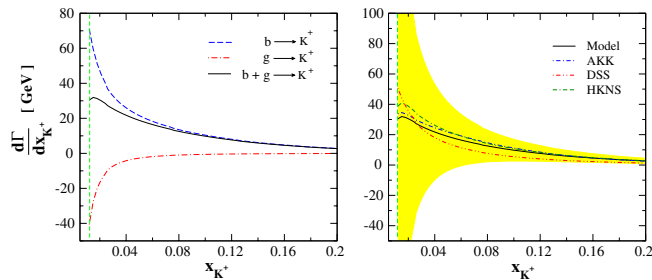


FIG. 19 (color online). Left panel: Energy distribution of the K^+ meson in top decay considering the fragmentation contribution of the b quark (dashed line) and gluon (dot-dashed line) into the K^+ and the total contribution (solid line) at $\mu_F = m_t$. Right panel: Energy distribution and its uncertainty of K^+ considering the FFs obtained by our model, AKK, DSS and HKNS [23,24,28].

$x_H = 2m_H/(m_t^2 - m_W^2)$. For comparison, we also show the energy spectrum of light mesons in top decay using the FFs obtained by AKK, DSS, and HKNS in Figs. 18 and 19.

VI. CONCLUSIONS

We have determined the nonperturbative parton fragmentation functions for the pion and kaon in the LO and NLO approximations from a global analysis of single-inclusive electron-positron annihilation $e^+e^- \rightarrow (\gamma, Z) \rightarrow H + X$ and the double-spin asymmetry from semi-inclusive deep inelastic scattering data, $A_1^{N,H}$, $\vec{l}(l) + \vec{N} \rightarrow l'(l') + H + X$. Our analysis was based on the ZM-VFNS scheme, where all quarks are treated as massless particles. Our new parametrization form covers a wide kinematic range of z because of the extra term $[1 - e^{-\gamma_i z}]$, which controls the medium- z region and improves the accuracy of the global fit. Figures 1–5 show the comparison of our model with SIA and double-spin asymmetry SIDIS experimental data and indicate that our model is successful. We determined the

FFs of gluon and light quarks at the initial scale $\mu_0^2 = 1 \text{ GeV}^2$ and the FFs of heavy quarks at $\mu_0^2 = m_c^2$ and $\mu_0^2 = m_b^2$. The evaluation was performed using the DGLAP equations. The theoretical results of the b heavy quark for the pion in our model and other models such as HKNS and DSS [23,24] deviate from the SLD and DELPHI data at large z , and any deviation between theory and experimental data occurs a large χ^2 . In comparison with other groups we applied—for the first time—spin asymmetry data ($A_1^{N,H}$) in the global analysis of the fragmentation functions, and the energy scales reported for the SIDIS experimental data are low-energy scales which are usually smaller than the e^+e^- annihilation scales (see Tables V, VI, VII, and VIII). On the other hand, adding the SIDIS data in a global fit allows us to test the universality of parton fragmentation functions so that the results are in good agreement with the FFs of other models. We also used one of the most accurate polarized and unpolarized parton distribution functions, i.e., NLO DSSV for polarized PDFs and NLO KKT12 for unpolarized PDFs. Using PDFs to determine FFs both indicates the universality of PDFs and is a good test for perturbative QCD analysis. We also applied fragmentation functions to determine the parton distributions into the proton, deuteron, and neutron, and showed that parton densities do not depend on the corresponding cross sections and are universal. Finally, we used the fragmentation functions to predict the energy spectrum of π^+ and K^+ mesons produced in top-quark decay. The comparison of our results for the pion and kaon energy spectra with other models shows that the fragmentation functions are universal; see Figs. 18 and 19.

ACKNOWLEDGMENTS

We warmly acknowledge F. I. Olness, S. J. Brodsky, and G. Kramer for valuable discussions, critical remarks, and reading the manuscript. We appreciate E. Christova and M. Leitgab for useful suggestions and comments. A. N. K. thanks the Stanford Institute for Theoretical Physics for partial support and the Physics Department of Southern Methodist University for their hospitality during the completion of this work. A. N. K. and M. M. thank the CERN TH-PH division for its hospitality, where a portion of this work was performed. We thank the School of Particles and Accelerators, Institute for Research in Fundamental Sciences for financial support.

APPENDIX: FORTRAN CODE

A FORTRAN package containing our unpolarized fragmentation functions for the pion and kaon at LO and NLO can be found at <http://particles.ipm.ir/links/QCD.htm> [73], as Supplemental Material to this article [74], or obtained via email from the authors. These functions are interpolated using cubic splines in Q^2 and a linear interpolation in $\log(Q^2)$. The package includes an example program to illustrate the use of the routines.

- [1] V.N. Gribov and L.N. Lipatov, *Yad. Fiz.* **15**, 781 (1972) [*Sov. J. Nucl. Phys.* **15**, 438 (1972)]; G. Altarelli and G. Parisi, *Nucl. Phys.* **B126**, 298 (1977); Yu. L. Dokshitzer, *Zh. Eksp. Teor. Fiz.* **73**, 1216 (1977) [*Sov. Phys. JETP* **46**, 641 (1977)].
- [2] D. de Florian, G. A. Navarro, and R. Sassot, *Phys. Rev. D* **71**, 094018 (2005).
- [3] D. de Florian, R. Sassot, M. Stratmann, and W. Vogelsang, *Phys. Rev. D* **80**, 034030 (2009).
- [4] S. Kretzer, E. Leader, and E. Christova, *Acta Phys. Pol. B* **33**, 3743 (2002).
- [5] S. Kretzer, E. Leader, and E. Christova, *Eur. Phys. J. C* **22**, 269 (2001).
- [6] X. Artru, [arXiv:1001.1061](https://arxiv.org/abs/1001.1061).
- [7] X. Artru and J. Czyzewski, *Acta Phys. Polon. B* **29**, 2115 (1998).
- [8] D. Buskulic *et al.* (ALEPH collaboration), *Z. Phys. C* **66**, 355 (1995); R. Barate *et al.*, *Phys. Rep.* **294**, 1 (1998).
- [9] P. Abreu *et al.* (DELPHI collaboration), *Eur. Phys. J. C* **5**, 585 (1998).
- [10] P. Abreu *et al.* (DELPHI collaboration), *Nucl. Phys.* **B444**, 3 (1995).
- [11] R. Akers *et al.* (OPAL collaboration), *Z. Phys. C* **63**, 181 (1994).
- [12] K. Abe *et al.* (SLD collaboration), *Phys. Rev. D* **69**, 072003 (2004).
- [13] W. Braunschweig *et al.* (TASSO collaboration), *Z. Phys. C* **42**, 189 (1989).
- [14] H. Aihara *et al.* (TPC collaboration), *Phys. Rev. Lett.* **52**, 577 (1984); **61**, 1263 (1988).
- [15] R. Itoh *et al.* (TOPAZ collaboration), *Phys. Lett. B* **345**, 335 (1995).
- [16] J. P. Lees *et al.* (BABAR Collaboration), [arXiv:1306.2895](https://arxiv.org/abs/1306.2895).
- [17] M. Leitgab *et al.* (Belle Collaboration), *Phys. Rev. Lett.* **111**, 062002 (2013).
- [18] D. P. Anderle, F. Ringer, and W. Vogelsang, in Proceedings of the 3rd Workshop on the QCD Structure of the Nucleon (QCD-N'12) (Bilbao, Spain, 2012).
- [19] A. Jain, M. Procura, B. Shotwell, and W. J. Waalewijn, *Phys. Rev. D* **87**, 074013 (2013).
- [20] Studies on fragmentation functions are listed at <http://www.pv.infn.it/~radici/FFdatabase/>.
- [21] B. A. Kniehl, G. Kramer, and B. Potter, *Nucl. Phys.* **B582**, 514 (2000); **B597**, 337 (2001); J. Binnewies, B. A. Kniehl, and G. Kramer, *Z. Phys. C* **65**, 471 (1995); *Phys. Rev. D* **52**, 4947 (1995); **53**, 3573 (1996); S. Albino, B. A. Kniehl, and G. Kramer, *Nucl. Phys.* **B725**, 181 (2005); **B734**, 50 (2006); B. A. Kniehl and G. Kramer, *Phys. Rev. D* **71**, 094013 (2005); **74**, 037502 (2006).
- [22] S. Kretzer, *Phys. Rev. D* **62**, 054001 (2000).
- [23] M. Hirai, S. Kumano, T.-H. Nagai, and K. Sudoh, *Phys. Rev. D* **75**, 094009 (2007).
- [24] D. de Florian, R. Sassot, and M. Stratmann, *Phys. Rev. D* **75**, 114010 (2007).
- [25] A. Airapetian *et al.* (HERMES Collaboration), *Phys. Rev. D* **71**, 012003 (2005).
- [26] M. Alekseev *et al.* (COMPASS Collaboration), *Phys. Lett. B* **680**, 217 (2009).
- [27] M. G. Alekseev *et al.* (COMPASS Collaboration), *Phys. Lett. B* **693**, 227 (2010).
- [28] S. Albino, B. A. Kniehl, and G. Kramer, *Nucl. Phys.* **B803**, 42 (2008).
- [29] R. K. Ellis, W. J. Stirling, and B. R. Webber, *QCD and Collider Physics* (Cambridge University Press, Cambridge, 1996).
- [30] J. C. Collins, *Phys. Rev. D* **58**, 094002 (1998).
- [31] B. A. Kniehl and G. Kramer, *Phys. Rev. D* **71**, 094013 (2005).
- [32] J. Binnewies, B. A. Kniehl, and G. Kramer, *Z. Phys. C* **65**, 471 (1995).
- [33] T. Kneesch, B. A. Kniehl, G. Kramer, and I. Schienbein, *Nucl. Phys.* **B799**, 34 (2008).
- [34] H. Khanpour, A. N. Khorramian, and S. A. Tehrani, *J. Phys. G* **40**, 045002 (2013).
- [35] A. N. Khorramian, S. Atashbar Tehrani, S. Taheri Monfared, F. Arbabifar, and F. I. Olness, *Phys. Rev. D* **83**, 054017 (2011).
- [36] M. Gluck, E. Reya, and A. Vogt, *Eur. Phys. J. C* **5**, 461 (1998).
- [37] C. Pisano, *Nucl. Phys. B, Proc. Suppl.* **191**, 35 (2009).
- [38] M. Gluck, C. Pisano, and E. Reya, *Eur. Phys. J. C* **50**, 29 (2007).
- [39] Y. Goto *et al.* (Asymmetry Analysis collaboration), *Phys. Rev. D* **62**, 034017 (2000); M. Hirai, S. Kumano, and N. Saito (Asymmetry Analysis Collaboration), *Phys. Rev. D* **69**, 054021 (2004).
- [40] E. Leader, A. V. Sidorov, and D. B. Stamenov, [arXiv:1007.4781](https://arxiv.org/abs/1007.4781).
- [41] D. de Florian, R. Sassot, M. Stratmann, and W. Vogelsang, *Phys. Rev. Lett.* **101**, 072001 (2008).
- [42] J. Blumlein and H. Bottcher, *Nucl. Phys.* **B841**, 205 (2010).
- [43] E. Leader, A. V. Sidorov, and D. B. Stamenov, *Phys. Rev. D* **82**, 114018 (2010).
- [44] M. Hirai and S. Kumano (Asymmetry Analysis Collaboration), *Nucl. Phys.* **B813**, 106 (2009).
- [45] A. N. Khorramian, A. Mirjalili, and S. A. Tehrani, *J. High Energy Phys.* **10** (2004) 062.
- [46] S. Atashbar Tehrani and A. N. Khorramian, *J. High Energy Phys.* **07** (2007) 048.
- [47] A. N. Khorramian, S. Atashbar Tehrani, S. Taheri Monfared, F. Arbabifar, and F. I. Olness, *Phys. Rev. D* **83**, 054017 (2011).
- [48] S. Atashbar Tehrani, A. N. Khorramian, S. Taheri Monfared, and F. Arbabifar, *AIP Conf. Proc.* **1374**, 391 (2011).
- [49] F. Arbabifar, A. N. Khorramian, S. Taheri Monfared, and S. Atashbar Tehrani, *Int. J. Mod. Phys. A* **26**, 625 (2011).
- [50] S. Taheri Monfared, A. Khorramian, S. Atashbar Tehrani, and Z. Haddadi, *Nucl. Phys. B, Proc. Suppl.* **210–211**, 125 (2011).
- [51] H. Khanpour and A. N. Khorramian, *Acta Phys. Pol. B* **41**, 2929 (2010).
- [52] S. Taheri Monfared, A. N. Khorramian, F. Arbabifar, and S. Atashbar Tehrani, *Acta Phys. Pol. B* **41**, 2921 (2010).
- [53] D. de Florian, M. Stratmann, and W. Vogelsang, *Phys. Rev. D* **57**, 5811 (1998).
- [54] A. A. Almasy, S. Moch, and A. Vogt, *Nucl. Phys.* **B854**, 133 (2012).
- [55] A. Mitov, S. Moch, and A. Vogt, *Phys. Lett. B* **638**, 61 (2006).

- [56] S. Albino and E. Christova, *Phys. Rev. D* **81**, 094031 (2010).
- [57] S. Albino, E. Christova, and E. Leader, [arXiv:1102.2305](https://arxiv.org/abs/1102.2305).
- [58] J. Binnewies, B. A. Kniehl, and G. Kramer, *Phys. Rev. D* **58**, 034016 (1998); M. Cacciari and M. Greco, *Nucl. Phys. B* **421**, 530 (1994).
- [59] A. D. Martin, R. G. Roberts, W. J. Stirling, and R. S. Thorne, *Eur. Phys. J. C* **28**, 455 (2003).
- [60] K. Nakamura (Particle Data Group), *J. Phys. G* **37**, 075021 (2010).
- [61] M. Soleymaninia, A. Khorramian, and M. Moosavi Nejad, *J. Phys. Conf. Ser.* **347**, 012017 (2012).
- [62] M. Soleymaninia, A. N. Khorramian, and S. M. Moosavinejad, *AIP Conf. Proc.* **1492**, 67 (2012).
- [63] M. Hirai and S. Kumano, *Prog. Theor. Phys. Suppl.* **186**, 244 (2010).
- [64] D. de Florian, R. Sassot, and M. Stratmann, *J. Phys. Conf. Ser.* **110**, 022045 (2008).
- [65] A. D. Martin, W. J. Stirling, R. S. Thorne, and G. Watt, *Eur. Phys. J. C* **63**, 189 (2009).
- [66] J. Pumplin, D. R. Stump, and W. K. Tung, *Phys. Rev. D* **65**, 014011 (2001).
- [67] M. Epele, R. Llubaroff, R. Sassot, and M. Stratmann, *Phys. Rev. D* **86**, 074028 (2012).
- [68] J. Pumplin, D. Stump, R. Brock, D. Casey, J. Huston, J. Kalk, H. L. Lai, and W. K. Tung, *Phys. Rev. D* **65**, 014013 (2001).
- [69] M. Hirai, S. Kumano, and N. Saito (Asymmetry Analysis Collaboration), *Phys. Rev. D* **69**, 054021 (2004).
- [70] S. Moch and P. Uwer, *Phys. Rev. D* **78**, 034003 (2008).
- [71] N. Cabibbo, *Phys. Rev. Lett.* **10**, 531 (1963); M. Kobayashi and T. Maskawa, *Prog. Theor. Phys.* **49**, 652 (1973).
- [72] B. A. Kniehl, G. Kramer, and S. M. M. Nejad, *Nucl. Phys. B* **862**, 720 (2012).
- [73] Program summary: <http://particles.ipm.ir/links/QCD.htm>.
- [74] See Supplemental Material at <http://link.aps.org/supplemental/10.1103/PhysRevD.88.054019> for a FORTRAN package containing our unpolarized fragmentation functions for the pion and kaon at LO and NLO. These functions are interpolated using cubic splines in Q^2 and a linear interpolation in $\log(Q^2)$. The package includes an example program to illustrate the use of the routines.